Molecular Therapy
Nucleic Acids
Original Article

Nanobody against SARS-CoV-2 non-structural protein Nsp9 inhibits viral replication in human airway epithelia

Tomas Venit,[1,6] Jeremy Blavier,[2,6] Sibusiso B. Maseko,[2,6] Sam Shu,[1] Lilia Espada,[3] Christopher Breunig,[3] Hans-Peter Holthoff,[3] Sabrina C. Desbordes,[3] Martin Lohse,[3] Gennaro Esposito,[1,4,5] Jean-Claude Twizere,[1,2] and Piergiorgio Percipalle[1,4]

[1]Division of Science and Mathematics, Biology Program, New York University Abu Dhabi, Abu Dhabi, United Arab Emirates; [2]Laboratory of Viral Interactomes, Unit of Molecular Biology of Diseases, GIGA Institute, University of Liege, Liège, Belgium; [3]ISAR Bioscience GmbH, Semmelweisstrasse 5, 82152 Planegg, Germany; [4]Center for Genomics and Systems Biology (CGSB), New York University Abu Dhabi, Abu Dhabi, United Arab Emirates; [5]Istituto Nazionale Biostrutture e Biosistemi (INBB), Roma, Italy

Nanobodies are emerging as critical tools for drug design. Several have been recently created to serve as inhibitors of severe acute respiratory syndrome coronavirus s (SARS-CoV-2) entry in the host cell by targeting surface-exposed spike protein. Here we have established a pipeline that instead targets highly conserved viral proteins made only after viral entry into the host cell when the SARS-CoV-2 RNA-based genome is translated. As proof of principle, we designed nanobodies against the SARS-CoV-2 non-structural protein (Nsp)9, which is required for viral genome replication. One of these anti-Nsp9 nanobodies, 2NSP23, previously characterized using immunoassays and nuclear magnetic resonance spectroscopy for epitope mapping, was expressed and found to block SARS-CoV-2 replication specifically. We next encapsulated 2NSP23 nanobody into lipid nanoparticles (LNPs) as mRNA. We show that this nanobody, hereby referred to as LNP-mRNA-2NSP23, is internalized and translated in cells and suppresses multiple SARS-CoV-2 variants, as seen by qPCR and RNA deep sequencing. These results are corroborated in three-dimensional reconstituted human epithelium kept at air-liquid interface to mimic the outer surface of lung tissue. These observations indicate that LNP-mRNA-2NSP23 is internalized and, after translation, it inhibits viral replication by targeting Nsp9 in living cells. We speculate that LNP-mRNA-2NSP23 may be translated into an innovative strategy to generate novel antiviral drugs highly efficient across coronaviruses.

INTRODUCTION

Coronaviruses that infect humans (HCoV) can be classified based on their pathogenicity into seasonal and highly pathogenic viruses. Seasonal viruses including HCoV-229E,[1] HCoV-OC43,[2] HCoV-NL63,[3] and HCoV-HKU1,[4] induce mild upper respiratory tract symptoms responsible for up to 30% of common colds in adults but in infants, the elderly, and immunocompromised individuals, can cause a severe lower respiratory tract disease.[5,6] The second category comprises severe acute respiratory syndrome virus (SARS)-CoV and SARS-CoV-2, as well as Middle East respiratory syndrome (MERS)-CoV, which can rapidly spread from the upper respiratory epithelial cells, infect the lower respiratory tract and induce severe diseases.[7] These viruses can cause epidemics and global pandemics such as coronavirus disease 2019 (COVID-19).[8,9] Coronaviruses, similarly to other viruses, have the potential to mutate and recombine to generate new variants that could escape currently available vaccines. It is, thus, of utmost importance to develop novel antiviral molecules targeting conserved processes of coronavirus replication, such as the conserved replication-transcription complex (RTC). The precise strategy used by coronaviruses to effectively replicate their large genome is not fully understood,[10,11] but the stability and proper organization of all components of coronaviruses-encoded RTC, including the RNA-dependent RNA polymerase and associated factors, play crucial roles in viral mRNAs synthesis from their RNA templates.[10,12] Structural snapshots of the SARS-CoV-2 RTC have been reported at atomic resolution. The mini RTC complex is assembled by several non-structural proteins (Nsp) including Nsp7-2xNsp8-Nsp12-2xNsp13 and the RNA-binding protein, Nsp9, necessary for RTC function.[13] Although Nsp9 has a strong tendency to oligomerize,[14–17] within the RTC, it is primarily a monomer.[18] Previous evidence linking Nsp9 dimerization and viral propagation[19–21] is well explained by the coincidence of all Nsp9 dimerization interface residues with its

Received 18 October 2023; accepted 12 August 2024;
https://doi.org/10.1016/j.omtn.2024.102304.

[6]These authors contributed equally

Correspondence: Jean-Claude Twizere, Division of Science and Mathematics, Biology Program, New York University Abu Dhabi, Abu Dhabi, United Arab Emirates.
E-mail: jean-claude.twizere@uliege.be
Correspondence: Piergiorgio Percipalle, Division of Science and Mathematics, Biology Program, New York University Abu Dhabi, Abu Dhabi, United Arab Emirates.
E-mail: pp69@nyu.edu

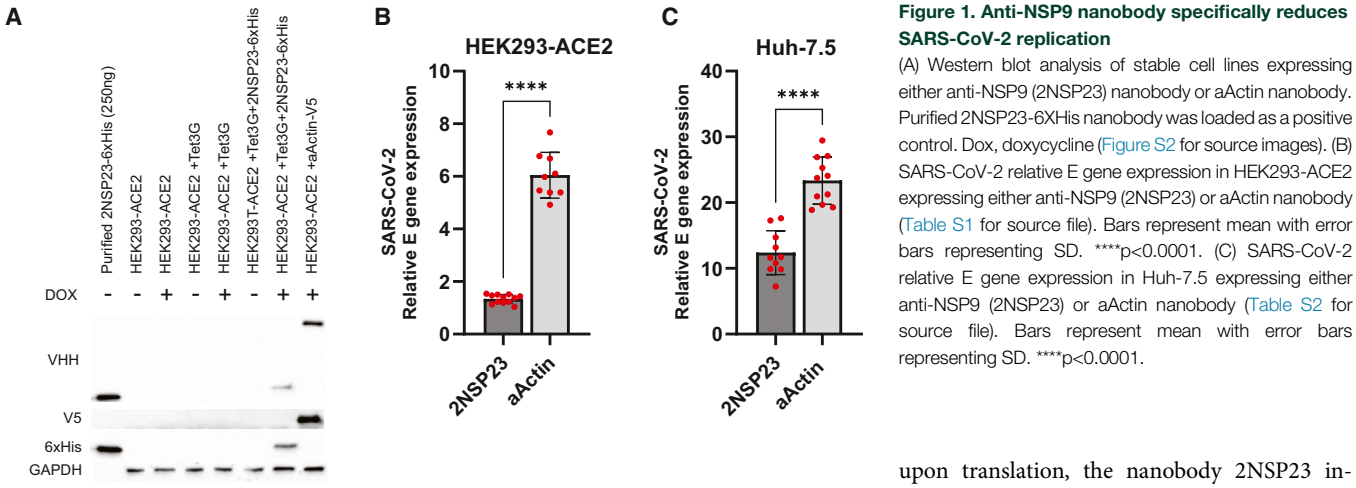

Figure 1. Anti-NSP9 nanobody specifically reduces SARS-CoV-2 replication

(A) Western blot analysis of stable cell lines expressing either anti-NSP9 (2NSP23) nanobody or aActin nanobody. Purified 2NSP23-6XHis nanobody was loaded as a positive control. Dox, doxycycline (Figure S2 for source images). (B) SARS-CoV-2 relative E gene expression in HEK293-ACE2 expressing either anti-NSP9 (2NSP23) or aActin nanobody (Table S1 for source file). Bars represent mean with error bars representing SD. ****p<0.0001. (C) SARS-CoV-2 relative E gene expression in Huh-7.5 expressing either anti-NSP9 (2NSP23) or aActin nanobody (Table S2 for source file). Bars represent mean with error bars representing SD. ****p<0.0001.

binding contacts in the catalytic center of the RNA-dependent RNA polymerase Nsp12.[18] Even the higher affinity for single-stranded RNA of Nsp9 dimers compared with monomers[21,22] did not support a functional homodimeric state because of the relative weakness of the binding,[23] suggesting the occurrence of a replication complex[20] well ahead the actual observation. Due to its unique role in viral RNA transcription, the Nsp9 protein could, therefore, serve as a compelling target for inhibiting coronavirus replication.

Several nanobodies have been generated against the surface-exposed spike protein to primarily block viral entry in the host cell.[24–28] However, given the frequency of mutations that affect spike, the efficiency of these nanobodies as potential antivirals is questionable. We, therefore, reasoned that the conserved Nsp9 would be a more efficient target to design novel compounds that robustly inhibit SARS-CoV-2 replication with the potential to work as pan-coronavirus antivirals. We generated 136 unique nanobodies against Nsp9 and the most promising ones, namely 2NSP23 and 2NSP90, were expressed, purified, and characterized.[14,15] The results from immunoassays show that these nanobodies effectively and specifically recognize viral Nsp9 in saliva samples from COVID-19 patients. Nuclear magnetic resonance (NMR) analysis and molecular dynamics simulations identified the epitopes on the wild-type Nsp9 protein recognized by the anti-NSP9 nanobodies and revealed that nanobody treatment leads to predominant non-functional tetrameric assembly of Nsp9.[14,15]

In the present study, we therefore investigated whether the 2NSP23 nanobody either stably expressed in cells or as an mRNA encapsulated into LNPs specifically inhibits SARS-CoV-2 replication in infected cells. LNPs containing mRNA coding for 2NSP23 nanobody, hereby referred to as LNP-mRNA-2NSP23, are internalized into cells where they are translated. Using a combination of techniques, we show that LNP-mRNA-2NSP23 protects cells and suppresses replication of several SARS-CoV-2 variants. Since nanobody 2NSP23 specifically binds to viral Nsp9,[15] these observations strongly suggest that, upon translation, the nanobody 2NSP23 inhibits viral replication by targeting Nsp9 in living cells. Given the conservation of Nsp9 across coronaviruses, we speculate that LNP-mRNA-2NSP23 or similar anti-NSP9 nanobody may be translated into an innovative technology to generate a pan-coronavirus antiviral drug.

RESULTS

Cellular expression of anti-Nsp9 2NSP23 nanobody specifically inhibits SARS-CoV-2 replication

To test whether 2NSP23 nanobody could affect the replication of SARS-CoV-2, we prepared the stable human embryonic kidney cell (HEK)293-ACE2 and Huh-7.5 cell lines with doxycycline-inducible expression of 2NSP23 nanobody fused to 6xHis tag. As a negative control, we prepared HEK293-ACE2 and Huh-7.5 cells expressing commercially available anti-actin (aActin) nanobody fused with a V5 tag.[29,30] We tested the expression of both nanobodies in these cells by western blot and showed that each nanobody is specifically expressed in each cell line and both of them have functional nanobody-specific VHH domains (Figure 1A). Next, we infected both cell lines with the SARS-CoV-2 virus and measured the expression of SARS-CoV-2 E gene expression 16 h after infection. In both cases, expression of nanobody 2NSP23 significantly reduced SARS-CoV-2 viral replication as evidenced by RT-qPCR quantification of E gene expression in comparison with aActin nanobody (Figures 1B and 1C).

Taken together, these results indicate that targeting SARS-CoV-2 NSP9 by expressing a specific nanobody 2NSP23 impairs SARS-CoV-2 replication.

The anti-Nsp9 2NSP23 nanobody mRNA is delivered as an LNP and expressed in human cells

We next tested an mRNA encapsulated into LNPs (mRNA-LNP) strategy[31,32] as an alternative method for delivery of nanobody-encoding molecules inside the cells. The mRNA-LNP is now accepted as a therapeutic platform after its successful use in SARS-CoV-2 mRNA vaccine designs,[33] and we hypothesize that this technology could also overcome the challenge of nanobody uptake into cells. We thus prepared mRNA molecules encoding a nanobody against

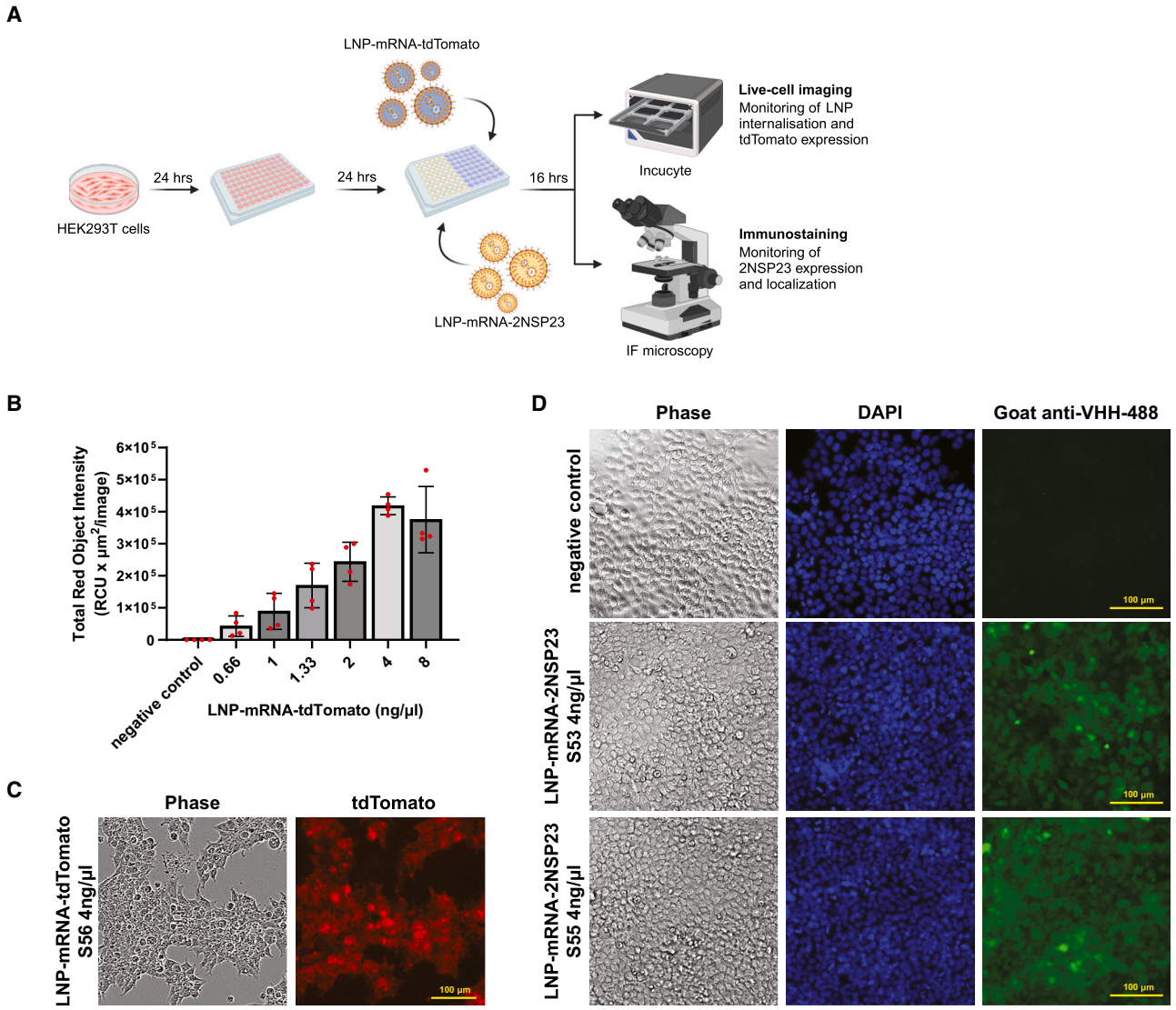

Figure 2. Testing of LNP-mRNA internalization and translation into a functional protein

(A) Experimental pipeline of LNP-mRNA treatment and readouts done for the HEK293T cells. (B) Quantification of tdTomato red signal intensity by the Incucyte at 16 h post-treatment with different dilutions of LNP-mRNA-tdTomato (Table S3 for source file). Bars represent mean with error bars representing SD. (C) Representative images of tdTomato expression by the Incucyte at 16 h post-treatment with LNP-mRNA-tdTomato S56 1:50. (D) Immunofluorescent staining of the anti-NSP9 nanobody at 16 h post-treatment with LNP-mRNA-2NSP23 S53 1:50 and S55 1:50.

SARS-CoV-2 NSP9 protein by *in vitro* transcription, which were encapsulated into LNPs by nano-assembly microfluidic mixing technology, as previously described.[34,35] This preparation is referred to as "LNP-mRNA-2NSP23." We used LNP encapsulating tdTomato mRNA as a negative control, allowing fluorescent monitoring of the efficiency of LNP-mRNA uptake by cells and subsequent translation into a functional protein. Subsequently, HEK293T cells were treated with LNP-mRNA-tdTomato or LNP-mRNA-2NSP23 for 24 h and monitored with the Incucyte live-imaging technology or fluorescent microscope upon immunostaining, respectively (Figure 2A). To test the optimal dilution of LNP-mRNAs for successful cellular uptake and translation, dilutions (1:25 to 1:300) from a stock concentration of 200 ng/µL mRNA. LNP-mRNA-tdTomato was used and the red fluorescent signal of tdTomato protein was analyzed 16 h after treatment (Figure 2B). We observed an increasing number of tdTomato-positive HEK293T cells with a peak at 4 ng/µL mRNA concentration (Figure 2B) with variable expression intensity of the tdTomato protein (Figure 2C). For LNP-mRNA-2NSP23, we tested two different batches (S53 and S55) both at 4 ng/µL mRNA concentration for 16 h on HEK293T cells, and stained the nanobody proteins using an Alexa Flour 488-conjugated anti-alpaca VHH antibody (Figure 2D). We observed batch-to-batch variability, but both

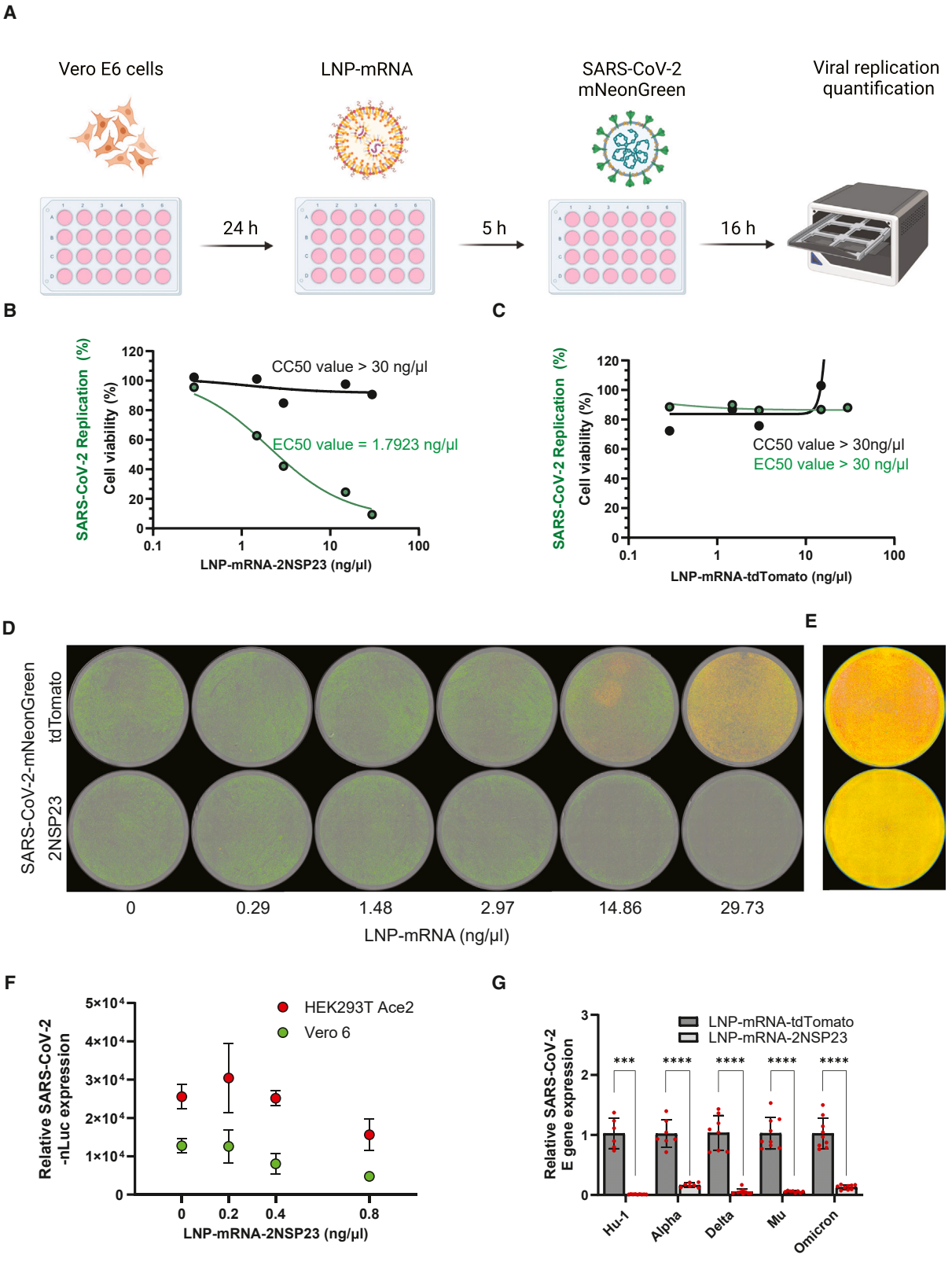

(legend on next page)

LNP-mRNA-2NSP23 were able to efficiently deliver the mRNA translated into protein in HEK293T cells (Figure 2D).

We conclude that the LNP technology is a suitable delivery method for cellular uptake of mRNA molecules encoding nanobodies and can be used as a general strategy for intracellular targeting of Nsp9 in cells infected with SARS-CoV-2.

Intracellular LNP-mRNA-2NSP23 expression leads to SARS-CoV-2 inhibition

Our initial experiments using lentiviral transduction showed that HEK293-ACE2 or Huh-7.5 cells stably expressing 2NSP23 nanobody exhibit less SARS-CoV-2 replication compared with control cells. To evaluate the ability of our LNP-mRNA-2NSP23 nanobody to affect viral replication, we established a pipeline with different live infectious coronaviruses (Figure 3A). VeroE6 cells treated with serial dilutions of LNP-mRNA-2NSP23 or LNP-mRNA-tdTomato were subsequently infected by an infectious recombinant clone (icSARS-CoV-2) that expresses the mNeonGreen as a reporter.[36] The results showed that treatment with LNP-mRNA-2NSP23 remarkably inhibited viral replication in a dose-dependent manner without affecting the cell viability (Figures 3B, 3D, and 3E). Using the variable slope model in GraphPad Prism software, we calculated the concentration of LNP-mRNA-2NSP23 at which the green fluorescence intensity, reflecting viral replication, is reduced to half of its maximal value (EC_{50}) and obtained 1.8 ng/μL of mRNA encoding 2NSP23 nanobody while cell viability (cytotoxicity concentration [CC_{50}] value > 30 ng/μL) is not affected by nanobody expression in cells (Figure 3B), on par with previously obtained results using the Food and Drug Administration/European Medicines Agency-approved antiviral small molecule Remdesivir.[37] In contrast, mRNA encoding tdTomato expression did not affect viral replication (Figures 3C–3E), nor cell viability (cytotoxicity concentration – CC_{50} value > 30 ng/μL). We next used an independent recombinant infectious SARS-CoV-2 clone, harboring the nanoluciferase as a reporter marker.[38] In two cell lines, VeroE6 and HEK293-ACE2, we observed a dose-dependent decrease in relative nano-luciferase values when cells were treated with LNP-mRNA-2NSP23 targeting NSP9 protein (Figure 3F). Data are normalized to cell viability to control for any inherent toxicity of LNP-mRNA formulations.[39]

To find out whether LNP-mRNA-2NSP23 treatment inhibits replication of different SARS-CoV-2 variants, HEK293-ACE2 cells treated with LNP-mRNA-2NSP23 or LNP-mRNA-tdTomato, respectively, were infected with the wild-type SARS-CoV-2 Hu-1 and SARS-CoV-2 variants Alpha, Delta, Mu and Omicron. RT-qPCR analysis of viral E gene expression shows that LNP-mRNA-2NSP23 (mRNA concentration = 0.4 ng/μL) was able to significantly abrogate viral replication of all variants in comparison to LNP-mRNA-tdTomato treated samples (Figure 3G).

Taken altogether, these results indicate that mRNA molecules encoding the 2NSP23 nanobody are delivered into cells and are translated into fully functional nanobodies that target SARS-CoV-2 Nsp9 and inhibit viral replication.

2NSP23 nanobody treatment rescues transcriptional changes induced by SARS-CoV-2 infection

While facilitating viral replication by contributing to RTC assembly, SARS-CoV-2 Nsps, including Nsp9 and Nsp14, directly affect the host cell transcriptome.[40] In this way, SARS-CoV-2 has a direct effect on the transcriptional profile of infected cells.[41–44] We, therefore, tested whether treatment of HEK293T-ACE2 cells with the 2NSP23 nanobody rescues changes in host cell gene expression due to SARS-CoV-2 infection. Cells treated with LNP-mRNA-2NSP23 or LNP-mRNA-tdTomato were infected with SARS-CoV-2 variants Alpha, Delta, Omicron, and Mu, and total RNA was isolated from all samples and subjected to deep RNA sequencing (RNA-seq). The sequencing reads were then aligned to human and SARS-CoV-2 genomes to measure the overall contribution of SARS-CoV-2 reads to total reads (Figure 4A). As expected, non-infected cells (NCs) did not contain any SARS-CoV-2 RNA reads, while in infected cells SARS-CoV-2 reads contributed to approximately 25%–50% of total reads, depending on the SARS-CoV-2 variant in control LNP-mRNA-tdTomato-treated cells. In contrast, LNP-mRNA-2NSP23 treatment significantly decreased the SARS-CoV-2 reads contribution to the total reads ratio in all variants, further confirming that SARS-CoV-2 RNA replication is inhibited upon nanobody treatment. Next, we performed hierarchical clustering based on the similarity of all SARS-CoV-2-positive and -negative samples treated with either LNP-mRNA-2NSP23 or LNP-mRNA-tdTomato (Figure 4B). We found that all LNP-mRNA-2NSP23-treated samples, regardless of

Figure 3. Inhibition of SARS-CoV-2 replication by LNP-mRNA-2NSP23

(A) Experimental pipeline for testing the LNP-mRNA effect on SARS-CoV-2 replication. (B) Vero E6 cells treated with serial dilution (29.7, 14.86, 2.97, 1.48, and 0.29 ng/μL) of LNP-mRNA-2NSP23 were infected with SARS-CoV-2-mNeonGreen, and green fluorescence and cell viability were quantified using Incucyte S3 imaging (Table S4 for source file). (C) Vero E6 cells treated with serial dilution (29.7, 14.86, 2.97, 1.48, and 0.29 ng/μL) of LNP-mRNA-tdTomato were infected with SARS-CoV-2-mNeonGreen, and green fluorescence and cell viability were quantified using Incucyte S3 imaging (Table S5 for source file). (D) Representative images from Incucyte S3 imaging system. The green color corresponds with the SARS-CoV-2-mNeonGreen-positive cells. The gradual yellow color indicates a concomitant expression of mNeonGreen (green) and tdTomato (red), respectively. (E) 16-color LUT transformation of the green channel (subtracting the signal from tdTomato) of the same Innucyte S3 Image showing only the SARS-CoV-2-mNeonGreen infected cells treated with 29.73 ng/μL of LNP-mRNAs in Figure 3D. The red color represents the SARS-CoV-2 positive cells. (F) Vero E6 (green) or HEK293-ACE2 (red) treated with the indicated concentration of LNP-mRNA-2NSP23 were infected with a SARS-CoV-2-nLuc viral strain and luciferase expression was quantified 24 h pi. Nano-luciferase values are normalized using control cells treated with LNP-mRNA-2tdTomato (Table S6 for source file). Dots represent mean with error bars representing SD. (G) HEK293-ACE2 cells treated with either 0.4 ng/μL of LNP-mRNA-2NSP23 or LNP-mRNA-tdTomato were infected with indicated SARS-CoV-2 viral strains. The SARS-CoV-2 E gene expression was quantified by qPCR and normalized to the control LNP-mRNA-tdTomato treated cells (Table S7 for source file). Bars represent mean with error bars representing SD. ***p<0.001, ****p<0.0001.

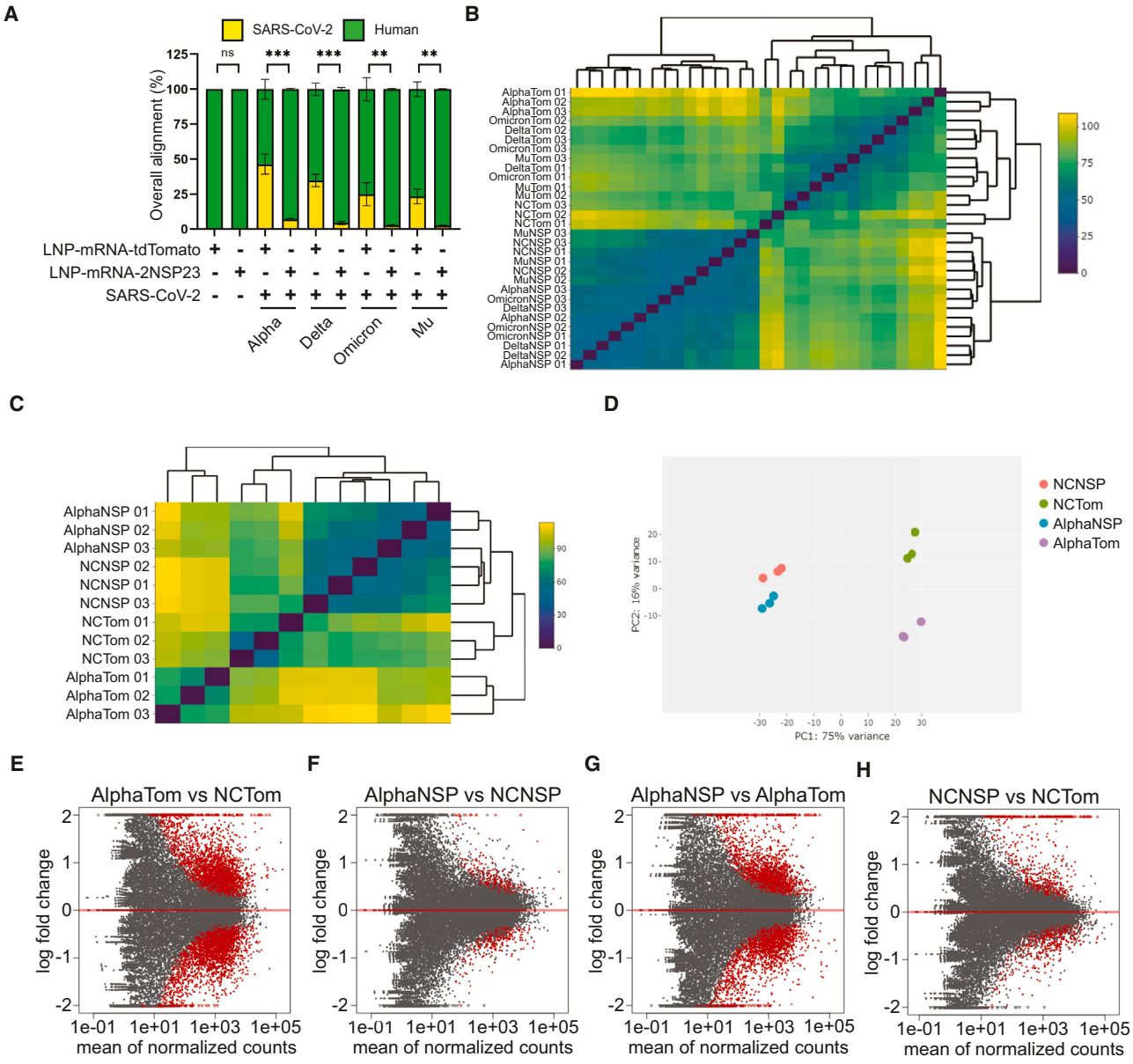

Figure 4. Nanobody treatment leads to a specific differential gene expression and suppression of SARS-CoV-2 replication

(A) Overall alignment of sequencing reads to SARS-CoV-2 and human genomes in samples treated with LNP-mRNA-2NSP23 or LNP-mRNA-tdTomato in non-infected or SARS-CoV-2-infected cells. Bars represent mean with error bars representing SD. **p < 0.01, ***p<0.001, ns (not significant). (B) A heatmap representation of the distance matrix clustering based on similarity between all experimental samples. (C) A heatmap representation of the distance matrix clustering based on similarity between non-infected (NC) and SARS-CoV-2 Alpha variant-infected (Alpha) cells treated either with LNP-mRNA-2NSP23 (NSP) or LNP-mRNA-tdTomato (Tom). (D) Principal component analysis plot of non-infected and SARS-CoV-2 Alpha variant-infected cells treated either with LNP-mRNA-2NSP23 or LNP-mRNA-tdTomato. (E) MA plot showing differential gene expression between SARS-CoV-2 infected (AlphaTom) and non-infected (NCTom) cells treated with LNP-mRNA-tdTomato. Each red dot represents a single DEG with up-regulated genes in the upper part of the MA lot and down-regulated genes in lower part of the MA plot. (F) MA plot showing differential gene expression between SARS-CoV-2 infected (AlphaNSP) and non-infected (NCNSP) cells treated with LNP-mRNA-2NSP23. Each red dot represents a single DEG with up-regulated genes in the upper part of the MA lot and down-regulated genes in lower part of the MA plot. (G) MA plot showing differential gene expression between SARS-CoV-2 infected cells treated with LNP-mRNA-2NSP23 (AlphaNSP) or control LNP-mRNA-tdTomato (AlphaTom). Each red dot represents a single DEG with up-regulated genes in the upper part of the MA lot and down-regulated genes in lower part of the MA plot. (H) MA plot showing differential gene expression between NCs treated with LNP-mRNA-2NSP23 (NCNSP) or treated with LNP-mRNA-tdTomato (NCTom). Each red dot represents a single DEG with up-regulated genes in the upper part of the MA lot and down-regulated genes in lower part of the MA plot.

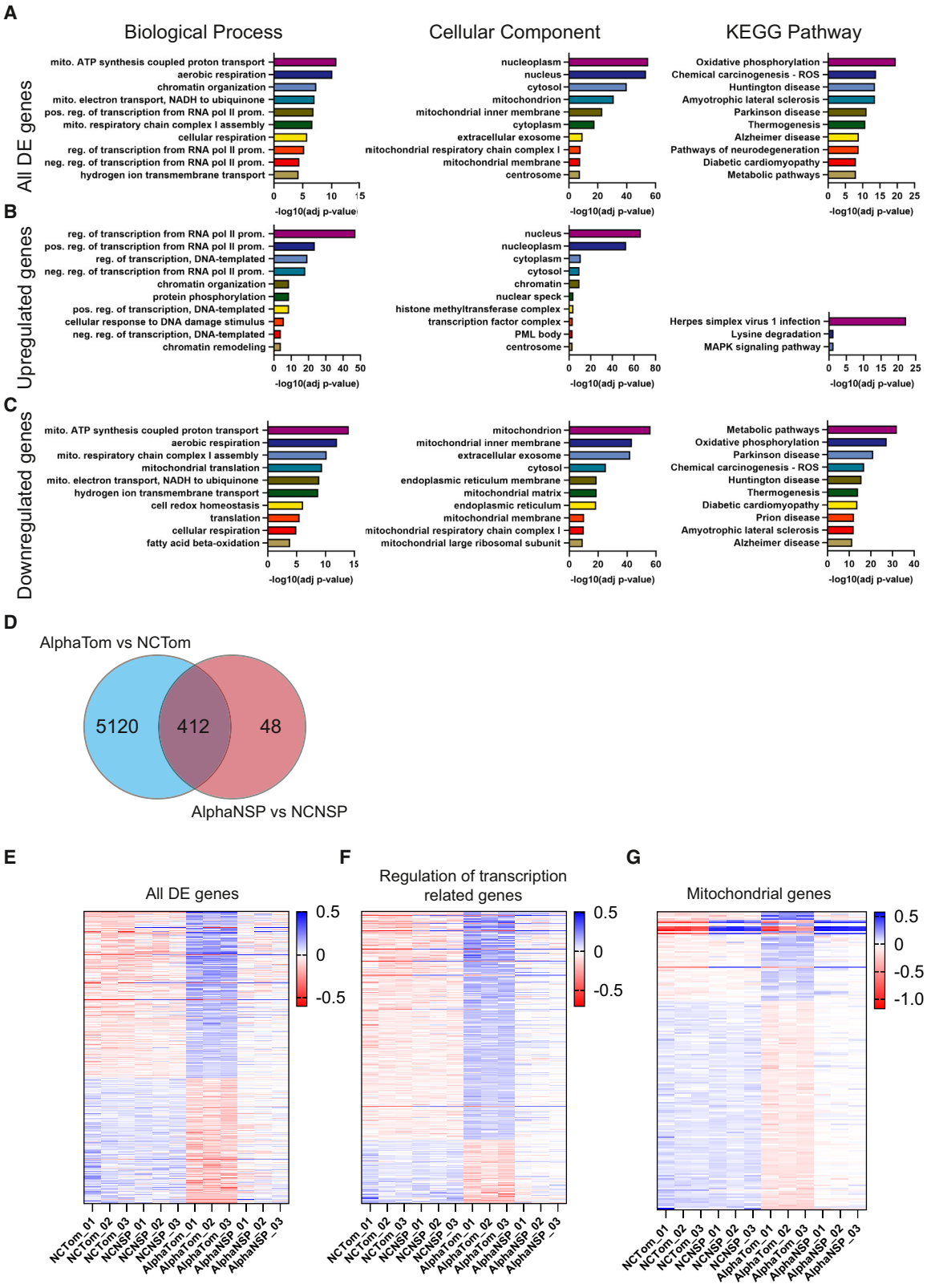

(legend on next page)

their infection status, randomly clustered, while LNP-mRNA-tdTomato-treated samples were separated based on SARS-CoV-2 positivity, which indicates that LNP-mRNA-2NSP23 treatment suppresses the transcriptional effect of SARS-CoV-2 infection (Figure 4B). The Alpha variant showed the greatest impact on transcriptional profiling, with a clear separation between the SARS-CoV-2-infected LNP-mRNA-tdTomato-treated cells in comparison with the rest of the samples. Therefore, we next performed hierarchical clustering of RNA reads obtained from NCs or SARS-CoV-2 Alpha variant-infected cells (Alpha), which were simultaneously treated with either LNP-mRNA-2NSP23 (NSP) or LNP-mRNA-tdTomato (TOM) (Figure 4C). Interestingly, this clustering is not seen in the principal component analysis, where samples are separated based on the treatment and infection status (Figure 4D). However, even here the variance between infected and non-infected samples in LNP-mRNA-2NSP23-treated cells is lower than in LNP-mRNA-tdTomato-treated cells. The big variance between LNP-mRNA-2NSP23 and LNP-mRNA-tdTomato-treated cells suggests that the expression of the 2NSP23 nanobody in cells causes a specific transcriptional response in cells (Figure 4D). To understand these differences, we performed pairwise comparisons between the four conditions to identify differentially expressed genes (DEGs) (Figures 4E–4H). The MA plots obtained from this analysis show statistically significant DEGs (in red), which are either up-regulated (upper part) or down-regulated (lower part) in the first condition in comparison with o the second condition. Figure 4E shows the effect of SARS-CoV-2 infection on LNP-mRNA-tdTomato-treated cells with 2,862 up- and 2,668 down-regulated genes. In contrast, SARS-CoV-2 infection has only a marginal effect on LNP-mRNA-2NSP23 treated cells with only 219 up- and 241 down-regulated genes (Figure 4F). The comparison between SARS-CoV-2-infected cells treated with LNP-mRNA-2NSP23 or LNP-mRNA-tdTomato shows similar pattern and number of DEGs (2,003 up- and 2,023 down-regulated), as seen between infected and non-infected LNP-mRNA-tdTomato-treated samples, suggesting that LNP-mRNA-2NSP23 expression in the cells suppresses the transcriptional outcome of viral infection to almost non-infected levels (Figure 4G). Finally, the comparison between the treatments in NCs shows the DEGs whose expression directly depends on LNP-mRNA-2NSP23 treatment with 460 genes to be up-regulated and 271 genes to be down-regulated (Figure 4H). In conclusion, transcriptional profiling of SARS-CoV-2-infected cells treated with either LNP-mRNA-2NSP23 or LNP-mRNA-tdTomato supports our previous results showing the specific role of anti-NSP9 nanobodies in the reduction of viral replication.

2NSP23 nanobody treatment rescues mitochondrial function and activates antiviral immune response

During infection, SARS-CoV-2 hijacks the cellular transcription machinery and suppresses mitochondria-dependent innate immune response to produce viral proteins.[45–48] We performed Gene Ontology (GO) analyses of all DEGs between SARS-CoV-2 infected and NCs treated with control LNP-mRNA-tdTomato and focused on the top hits in "biological process," "cellular component," and "Kyoto Encyclopedia of Genes and Genomes (KEGG) pathway" GO terms to identify the most affected cellular processes, compartments, and pathways (Figure 5A). With almost no exceptions, the majority of GO terms in all three categories are associated with mitochondrial biogenesis and metabolism, as well as with the organization of chromatin structure and transcriptional regulation. To examine whether the affected pathways are activated or suppressed, we performed GO analysis on up-regulated or down-regulated genes separately (Figures 5B and 5C). Here, the GO terms associated with the regulation of transcription are heavily up-regulated (Figure 5B), while GO terms associated with mitochondrial function and oxidative phosphorylation are suppressed (Figure 5C), suggesting that LNP-mRNA-tdTomato has no significant effect on the SARS-CoV-2 virus, which fully hijacked cells for its replication and spreading. As LNP-mRNA-2NSP23 treatment heavily decreased the number of DEGs between SARS-CoV-2-infected cells and NCs, we next studied whether SARS-CoV-2 affects the same biological processes in nanobody-expressing cells. The comparison between the two datasets shows that the majority of DEGs observed in LNP-mRNA-2NSP23-treated samples overlap with DEGs in LNP-mRNA-tdTomato-treated samples upon SARS-CoV-2 infection (Figure 5D). We performed the same GO analysis for these genes and found that both regulation of transcription and mitochondrial function are affected in LNP-mRNA-2NSP23-treated samples, but to a significantly lower extent (Figures S1A–S1C; Tables S22–S24). To see how nanobody treatment affects the expression of individual genes, we took all DEGs between SARS-CoV-2-infected cells and NCs treated with LNP-mRNA-tdTomato and plotted normalized read counts for each gene and each

Figure 5. SARS-CoV-2 virus infection leads to differential gene expression of RNA Polymerase II transcription-regulatory genes and mitochondrial genes

(A) Top 10 GO terms associated with "biological process," "cellular component," and "KEGG pathway" groups based on the analysis of all DEGs between infected and uninfected cells treated with LNP-mRNA-tdTomato (AlphaTom vs. NCTom) (Table S8 for source file). (B) Top GO terms associated with "biological process," "cellular component" and "KEGG pathway" groups based on the analysis of only up-regulated genes in infected cells treated with LNP-mRNA-tdTomato in comparison with uninfected cells treated with LNP-mRNA-tdTomato (Table S9 for source file). (C) Top GO terms associated with "biological process," "cellular component," and "KEGG pathway" groups based on the analysis of only down-regulated genes in infected cells treated with LNP-mRNA-tdTomato in comparison with uninfected cells treated with LNP-mRNA-tdTomato (Table S10 for source file). (D) Venn diagram showing the number of specific and common genes that are DE upon SARS-CoV-2 infection in cells treated with LNP-mRNA-tdTomato (AlphaTom vs. NCTom) and SARS-CoV-2 infection in cells treated with LNP-mRNA-2NSP23 (AlphaNSP vs. NCNSP). (E) Gene expression heatmap of normalized counts for each DEG between infected and uninfected cells treated with LNP-mRNA-tdTomato (AlphaTom vs. NCTom) across each sample replicate (Table S11 for source file). (F) Gene expression heatmap of normalized counts for each DEG associated with GO term "Regulation of Pol II transcription" between infected and uninfected cells treated with LNP-mRNA-tdTomato (AlphaTom vs. NCTom) across each sample replicate (Table S12 for source file). (G) Gene expression heatmap of normalized counts for each DEG associated with GO term "Mitochondria" between infected and uninfected cells treated with LNP-mRNA-tdTomato (AlphaTom vs. NCTom) across each sample replicate. Data available as a Source data file (Table S13 for source file).

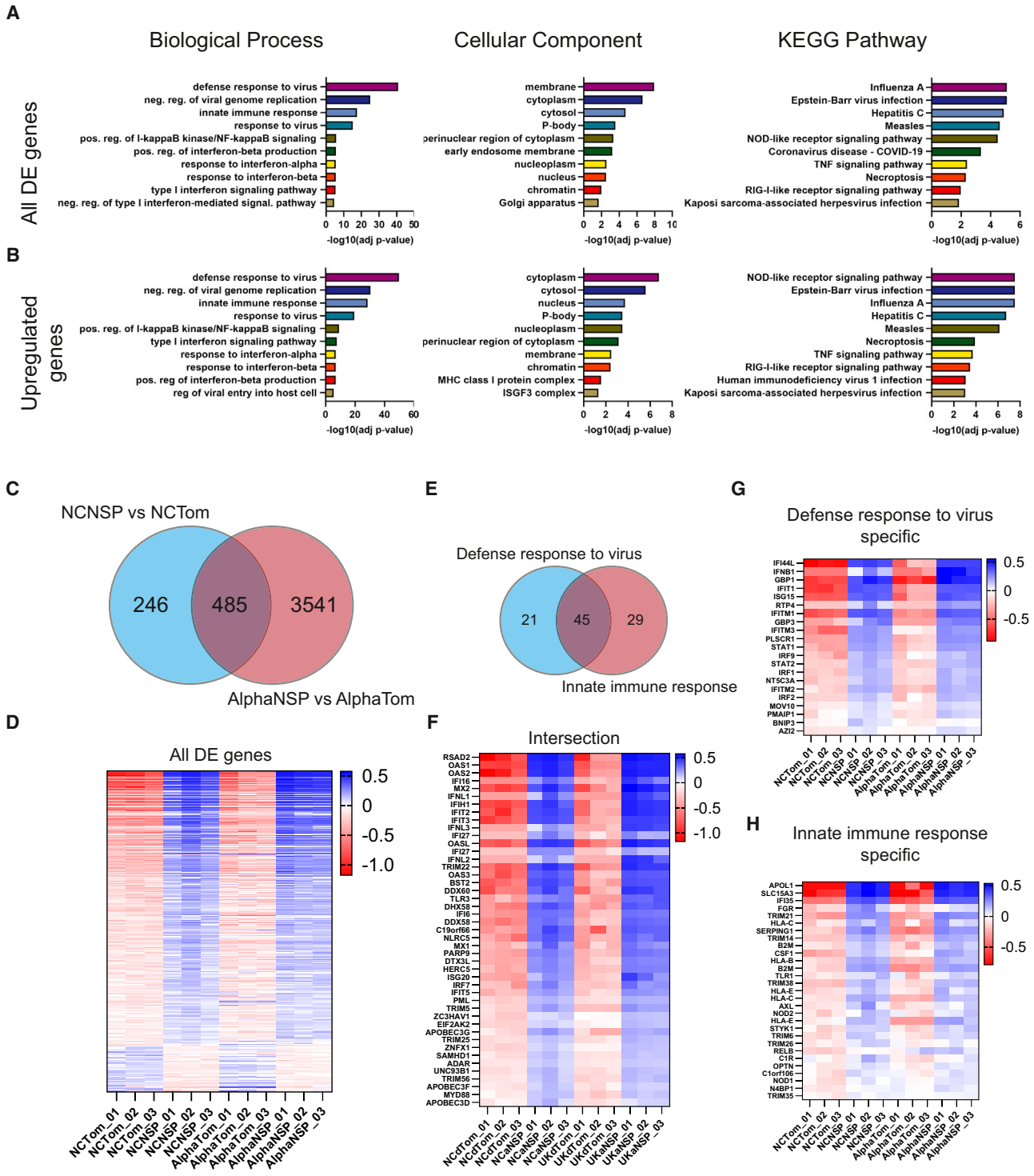

Figure 6. Nanobody treatment induces changes in gene expression related to the host antiviral immune response regardless of the SARS-CoV-2 infection

(A) Top 10 GO terms associated with "biological process," "cellular component," and "KEGG pathway" groups based on the analysis of all DEGs between NCs treated either with LNP-mRNA-2NSP23 or LNP-mRNA-tdTomato (NCNSP vs. NCTom) (Table S14 for source file). (B) Top GO terms associated with "biological process," "cellular component," and "KEGG pathway" groups based on the analysis of all up-regulated genes in NCs treated with LNP-mRNA-2NSP23 in comparison to NCs treated with LNP-mRNA-tdTomato (Table S15 for source file). (C) Venn diagram showing the number of specific and common genes which are DE in LNP-mRNA-2NSP23 treated NCs in

(legend continued on next page)

experimental condition in descending order in the form of a heatmap (Figures 5E–5G). The results show that SARS-CoV-2 infection has a prominent effect on expression profiles in LNP-mRNA-tdTomato-treated cells, while treatment with LNP-mRNA-2NSP23 reduces not only the number of DEGs but also the level of expression of those genes which are significantly changed (Figure 5E). This can be seen more profoundly in selected groups of genes related to the regulation of transcription (Figure 5F) and mitochondrial function (Figure 5G) where nanobody treatment suppresses the effect of SARS-CoV-2 infection on the transcriptional profile of cells. We, therefore, conclude that intracellular expression of 2NSP23 nanobody heavily rescues host cell gene expression programs that are otherwise dysregulated upon SARS-CoV-2 infection.

Next, we explored the pathways directly affected by 2NSP23 nanobody expression. The GO analysis of all DEGs between LNP-mRNA-2NSP23- and LNP-mRNA-tdTomato-treated NCs revealed multiple biological processes pertinent to antiviral immune response to be over-represented, including defense response to virus, negative regulation of viral genome replication, and innate immune response, as well as several KEGG pathways associated with virus infection (Figure 6A). To see whether these processes are activated or suppressed in these cells, we performed a GO analysis of up-regulated and down-regulated genes separately. As the majority of DEGs between LNP-mRNA-2NSP23- and LNP-mRNA-tdTomato-treated cells are up-regulated, we did not get any significant GO terms for down-regulated genes and GO terms associated with only up-regulated genes copies the patterns seen in global DE analysis (Figure 6B). This indicates that introducing nanobodies into cells triggers the host immune response even before SARS-CoV-2 infection. To test whether immune system activation by nanobody treatment is persistent even after SARS-CoV-2 infection, we compared the DEGs between LNP-mRNA-2NSP23 and LNP-mRNA-tdTomato treatments in non-infected versus SARS-CoV-2 infected cells. We found that LNP-mRNA-2NSP23 treatment causes a very specific cellular response which is maintained and even strengthened upon virus infection (Figures 6C and 6D). Finally, to understand how the nanobody may activate an immune response, we compared the DEGs in the two most significant GO terms “defense response to virus” and “innate immune response” (Figure 6E) and plotted expression profiles of every single gene based on their specificity and expression pattern to common genes found in both groups (Figure 6F), genes found only in “defense response to virus” group (Figure 6G) and “innate immune response” specific group of genes (Figure 6H). While there is a subset of down-regulated genes upon LNP-mRNA-2NSP23 treatment (Figure 6D), all DEGs related either to defense response to virus or innate immune response are up-regulated suggesting very specific activation of antivirus response in 2NSP23 nanobody expressing cells. A remarkable observation is that treatment of cells with LNP-mRNA-2NSP23 elicited enrichment of genes related to defense response to viruses in uninfected cells. Several genes in immune signaling pathways were heavily up-regulated in these healthy samples. For example, RSAD2, OAS1, and OAS2, all of which are crucial components of interferon signaling pathways, were also found to be similarly affected by SARS-CoV-2 infection,[49] and their expression profiles in these treated samples resemble those in the infected cells (Figure 6F). Taken all together these findings suggest that that 2NSP23 protects cells from SARS-CoV-2 infection by triggering genes involved in the antiviral immune response.

2NSP23 nanobody treatment suppress SARS-CoV-2 viral replication in three-dimensional reconstituted human upper airway epithelium tissues

Finally, to test if LNP-mRNA-2NSP23 suppresses SARS-CoV-2 replication in human tissue, close to physiological conditions, we used three-dimensional (3D) reconstituted human upper airway epithelium tissues from healthy donors, which are grown at air-liquid interface (ALI) (MucilAir-pool, Epithelix, Switzerland). This system mimics the upper layer of the human epithelium and has been previously used as a human model for *in vivo* SARS-CoV-2 infection.[50–53] Briefly, the 3D tissues pre-treated with either LNP-mRNA-2NSP23 or LNP-mRNA-tdTomato were apically infected with the SARS-CoV-2 virus for 1 h. This was followed by incubation in an ALI environment for 48 or 96 h before the apical washes were collected for viral quantification. Next, we performed a qPCR analysis to monitor the expression of the SARS-CoV-2 E gene as a proxy for viral replication at both time points. Results from this analysis show that treatment with LNP-mRNA-2NSP23 expressing anti-NSP9 nanobody in comparison with tdTomato control significantly reduced SARS-CoV-2 E gene expression in a dose-dependent manner (Figures 7A and 7B). These findings support our previous results in different cellular models and further indicate that mRNA-2NSP23 could block viral replication ex-vivo under physiological conditions.

In summary, by targeting Nsp9 through a nanobody that is efficiently expressed via an mRNA encapsulated into LNPs, it is possible to block SARS-CoV-2 replication in cellular models as well as *ex vivo* in

comparison to LNP-mRNA-tdTomato uninfected cells (NCNSP vs. NCTom), and LNP-mRNA-2NSP23 treated SARS-CoV-2 infected cells in comparison to SARS-CoV-2 infected cells treated with LNP-mRNA-tdTomato (AlphaNSP vs. AlphaTom). (D) Gene expression heatmap of normalized counts for each DEG between LNP-mRNA-2NSP23 and LNP-mRNA-tdTomato-treated NCs (NCNSP vs. NCTom) across each sample replicate (Table S16 for source file). (E) Venn diagram showing the intersection of DEGs associated with GO terms “Defense response to virus” and “Innate immune response” in NCs treated with LNP-mRNA-2NSP23 or LNP-mRNA-tdTomato. (F) Gene expression heatmap of normalized counts for each DEG found in the intersection between GO terms “Defense response to virus” and “Innate immune response” in NCs treated with LNP-mRNA-2NSP23 or LNP-mRNA-tdTomato (Table S17 for source file). (G) Gene expression heatmap of normalized counts for each DEG specific for GO term “Defense response to virus” in NCs treated with LNP-mRNA-2NSP23 or LNP-mRNA-tdTomato (Table S18 for source file). (H) Gene expression heatmap of normalized counts for each DEG specific for GO term “Innate immune response” in NCs treated with LNP-mRNA-2NSP23 or LNP-mRNA-tdTomato (Table S19 for source file).

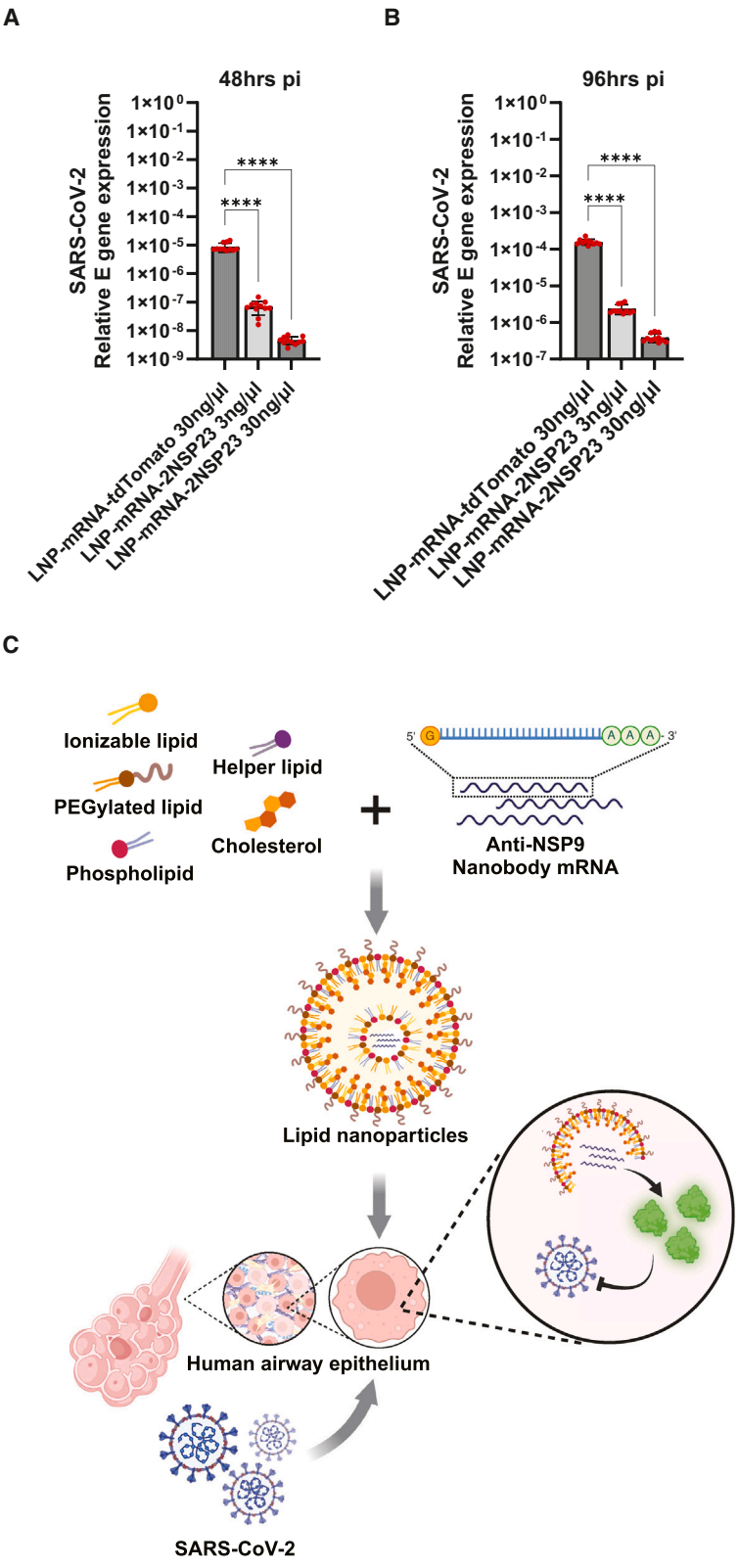

Figure 7. LNP-mRNA-2NSP23 blocks viral replication in 3D reconstituted human upper airway epithelium tissues in an air-liquid interphase environment

(A) Relative quantification of SARS-CoV-2 E gene expression in 3D reconstituted epithelium treated with either LNP-mRNA-2NSP23 or LNP-mRNA-tdTomato 48 h pi (Table S20 for source file). Bars represent mean with error bars representing SD. ****p<0.0001. (B) Relative quantification of SARS-CoV-2 E gene expression in 3D reconstituted epithelium treated with either LNP-mRNA-2NSP23 or LNP-mRNA-tdTomato 96 h pi (Table S21 for source file). Bars represent mean with error bars representing SD. ****p<0.0001. (C) Schematic view of nanobody-based therapy against SARS-CoV-2. mRNA coding for 2NSP23 nanobody against viral NSP9 is mixed with a combination of lipids to form mRNA encapsulated in LNPs. LNPs are internalized in cells and mRNA is released for translation into functional nanobody, which blocks viral replication in cells.

human nasal tissues, presumably by directly affecting the assembly and function of the viral RTC complex.

DISCUSSION

In this study, we have focused on the SARS-CoV-2 Nsp9 as a potential intracellular target to design compounds that might block the replication of coronaviruses. Specifically, we have established a pipeline for intracellular expression of 2NSP23, a novel nanobody that specifically interacts with both recombinantly expressed Nsp9 and the endogenous one in the saliva of COVID-19 patients.[15] Earlier work by NMR spectroscopy showed that anti-Nsp9 nanobodies, including both 2NSP23 and 2NSP90, stabilize a tetrameric/short oligomeric form of Nsp9.[14,15] As Nsp9 has been suggested to function in a monomeric/dimeric form to facilitate the assembly of the RTC complex, we speculated that targeting viral replication using 2NSP23 nanobody could serve as an inhibitor of viral replication that would affect the assembly of the RTC complex. To prove this hypothesis, we combined the use of 2NSP23 with RNA technology and LNPs. Using this approach, we show that 2NSP23 is efficiently delivered into HEK293T cells in the form of mRNA encapsulated into LNPs. After delivery, the 2NSP23 mRNA is intracellularly translated, binds to NSP9, and blocks SARS-CoV-2 infection in cells. Analysis of RNA-seq reads obtained from total RNA isolated from cells expressing the 2NSP23 nanobody and subjected to SARS-CoV-2 infection demonstrate the lack of viral RNA reads, indicating that replication of SARS-CoV-2 RNA is inhibited when Nsp9 is targeted by the nanobody. Nsp9 contributes to the assembly of RTC complexes at the genomic SARS-CoV-2 RNA genome, and this is an essential step in viral replication.[13,18] As endogenous Nsp9 seems to be quantitatively bound by 2NSP23, a likely mechanism of action leading to inhibition of viral RNA replication is a consequence of impaired RTC assembly due to the lack of Nsp9 availability.

Results from RNA-Seq experiments also indicate that in infected cells, 2NSP23 intracellular expression leads to a general rescue of the host cell transcriptional profile comparable to that of uninfected cells. This is particularly interesting considering the emerging view that viral proteins function in an orchestrated way to efficiently impact the host cell transcriptome after viral infection. For instance, expression of exogenous SARS-CoV-2 Nsp14 in cells has been shown to provoke a dramatic remodeling of the transcriptome similar to that observed after SARS-CoV-2 infection. Nsp14 seems to contribute to the remodeling of the transcriptome through a yet unclear mechanism that leads to alteration in the splicing of a set of genes and increased expression of circRNAs, all linked to innate immunity.[40] Our present work goes in the same direction; results from RNA-seq experiments show significant differential gene expression upon SARS-CoV-2 infection, especially of those genes involved in transcriptional regulation and mitochondrial functions. The GO term "Mitochondrion" seems to be the most impacted cellular component with metabolic pathways, especially oxidative phosphorylation, strongly down-regulated. This is consistent with previous studies showing that SARS-CoV-2 viral damage causes and intensifies oxidative stress.[54] More important, these mitochondrial genes involved in oxidative phosphorylation normally affected in infected cells were among those gene programs that were rescued in the presence of anti-Nsp9 nanobodies. Some of these genes include COX5B and NDUFS8, which are essential for the electron transport chain, and MRPL9, and MRPL24, as well as other candidates, which are mitochondrial ribosomal proteins that govern not only oxidative phosphorylation but also other cellular processes such as apoptosis and immune response. These results confirm that mitochondrial activity is a critical marker to examine if any treatment for the disease eventually works. It is remarkable that, by expressing the anti-Nsp9 nanobody intracellularly, we can rescue these gene expression programs. These results suggest a potential role of Nsp9 as well as other Nsp proteins such as Nsp14 not only in RTC assembly but also in altering the expression of cellular genes involved in essential host cell functions. How this is achieved remains to be understood. However, given that 2NSP23 expression rescues these gene programs, it is likely that Nsp9, being an RNA-binding protein, might interact with nuclear factors and directly affect gene expression at a transcriptional level in the host cells.[55] So, nanobody 2NSP23 is ideally suited to function as a potential antiviral against SARS-CoV-2 infection. Considering the extremely low degree of mutagenicity of Nsp9,[56] we propose that targeting Nsp9 and/or other Nsps could define a new strategy to combat related coronaviruses such as MERS and SARS-CoV. The remarkable finding that treatment of uninfected cells with 2NSP23 elicits enrichment of genes related to defense response to viruses also suggests a potentially much broader use of this nanobody in general prophylaxis against pathogens. The LNPs, the unmodified nanobody mRNA used in our study, and the translated llama-based nanobody could all potentially lead to unspecific immune response activation. However, we can exclude these possibilities for several reasons. First, the same composition of lipids was used for LNP preparation in testing and control conditions. Second, the negative control tdTomato mRNA is also unmodified, but does not trigger an immune response in all cells we tested in the present study. Finally, expression of an unrelated aActin nanobody in cells does not lead to a specific decrease in SARS-CoV-2 replication, suggesting that the use of a random nanobody does not trigger the immune response in cells which, in turn, supports a specific role of the anti-NSP9 nanobody 2NSP23. This agrees with other studies showing that llama-based nanobodies have, in general, very low immunogenicity and even non-humanized unmodified nanobodies show only marginal capacity to induce an immune response in humans.[57,58] Although the mechanisms underlying the specific role of 2NSP23 on immune system activation remain to be understood, we speculate that, by triggering the expression of genes involved in antiviral immune response, nanobody 2NSP23 protects cells from SARS-CoV-2 infection and, potentially, provides broadly neutralizing activity against coronaviruses and other pathogens.

In summary, engineering modified mRNA molecules encoding highly potent nanobodies directed against key components of the SARS-CoV-2 RTC components such as Nsp9 is an attractive strategy to inhibit SARS-CoV-2 RNA replication. An advantage of this approach is that it targets intracellular viral proteins that are less prone to mutations in comparison to cell surface expressed proteins such as the

spike proteins and therefore, they may provide innovative solutions to combat pathogens. In addition, because of the larger interface area between the nanobody and its target, it is also anticipated that these mRNA-nanobodies-based therapies should drive fewer resistant mutants compared with small molecules targeting catalytic pockets for instance within the Nsp12 enzyme. Translating those therapeutic mRNAs into innovative antivirals should thus follow the same path as current mRNA vaccines against SARS-CoV-2. Moreover, mRNA-nanobodies-based therapies in combination with LNPs also allow for easy virus-free delivery into cells *in vivo* as proposed by our study and other research focusing on the administration of such particles[59–62] or nanobodies themselves[63] via inhalation.

Study limitations

We provide proof-of-concept data that intracellularly expression of a nanobody targeting SARS-CoV-2 NSP9 protein leads to inhibition of viral replication in cellular models including *ex vivo* human 3D tissues. Future studies will focus on pre-clinical studies of small animal models such as Syrian hamsters and, if possible, non-human primates to determine the potential *in vivo* toxicity of systemic or local administration of optimized composition of LNP-mRNA-2NSP23. In addition, mRNA molecules used in this study were not modified to include, for example, N1-methyl pseudouridine which has been shown to increase mRNA stability and reduce innate immunity activation.[64] Finally, determining at which state of viral RNA synthesis the 2NSP23 nanobody binds to the RTC, and the potentially affected activity of NSP9 (NMPylation, RNAylation, and deRNAylation/capping) should allow a precise understanding of the molecular mode of replication inhibition, and the design of more potent inhibitors. This could be accomplished using Cryo-EM and existing RTC structures.[13,18,65]

METHODS

Cell culture

The HEK 293T cells, human embryonic kidney cells stably expressing the human ACE-2 receptor (HEK293-ACE2), human hepatocellular carcinoma cells (Huh-7.5), and epithelial cells from African green monkey *Cercopithecus aethiops* (Vero E6) cells were grown in full DMEM containing 10% fetal bovine serum, 100 U/mL penicillin, and 100 mg/mL streptomycin (Millipore-Sigma) in the humidified incubator at 37°C with 5% CO_2.

Preparation of stable cell lines expressing anti-NSP9 or aActin nanobodies

HEK293-ACE2 and Huh-7.5 cells with doxycycline-inducible expression of 2NSP23 nanobody were prepared by sequential transduction of cells with first, the lentivirus vector carrying hygromycin resistance and Tet regulatory protein Tet3G under CMV promoter (VectorBuilder) followed by a second round of transduction with lentivirus carrying neomycin resistance and 2NSP23 gene fused with 6xHis tag under Tre3G promoter (VectorBuilder). The HEK293-ACE2 and Huh-7.5 cells with stable expression of aActin nanobody expression were prepared by lentiviral transduction with a vector carrying neomycin resistance and aActin-nanobody gene fused with V5 tag and GFP[29,30] (VectorBuilder).

Cells were grown in a DMEM medium containing 10% fetal bovine serum, 100 U/mL penicillin, and 100 mg/mL streptomycin (Millipore-Sigma) in a humidified incubator with 5% CO_2 at 37°C. Expression of 2NSP23 nanobody was induced by doxycycline hyclate (500 ng/mL), which was added to media 48 h before the experiments. The same treatment was used in aActin nanobody-expressing cells to minimize the possible effects of doxycycline on the outcome of the experiment.

Western blot analysis

RIPA buffer (50 mM Tris-HCl pH 7.5, 150 mM NaCl, 1 mM EDTA, 1% NP-40, 0.5% sodium deoxycholate, and 0.1% SDS) containing 1× complete protease inhibitor cocktail (Roche) was used to collect total cellular lysates from HEK293-ACE2 cells. BCA protein assay kit (Thermo Fisher Scientific) was used to measure protein concentration and 20μg of total protein per sample together with 1× Laemmli buffer was loaded to an 18% SDS-PAGE gel and separated under reducing conditions. The separated proteins were transferred to a PVDF membrane, blocked with 3% milk in 1× TBST buffer (20 mM Tris pH 7.5, 150 mM NaCl, 0.1% Tween 20) for 1 h and immunoblotted with primary antibodies fused with horseradish peroxidase (HRP) overnight at 4°C in a rotator. The next day, the membranes were washed three times with 1× TBST, protein bands were developed with ECL western blot Substrate (BioRad), and western blots were imaged by a ChemiDoc MP Imaging system (BioRad). The antibodies used in the analysis were anti-V5-HRP (Abcam, ab1325), anti-GAPDH-HRP (Abcam, ab9484), anti-6xHis-HRP (Abcam, ab237339), and anti-VHH-HRP (Jackson Immuno Research, 128-035-230).

mRNA production

The 2NSP23 nanobody mRNA was prepared by *in vitro* transcription of a DNA molecule of using the HiScribe T7 mRNA Kit with CleanCap Reagent AG (New England BioLabs). The obtained mRNA has the following sequence and includes a 5′-CAP and a poly-A tail: aggaauugugagcggauaacaauucccucuagaauaauuuuguuuaacuuuaagaaggagauauaccaugggcaugcagCAGGUGCAGCUGCAGGAGUCUGGAGGAGGAUUGGUACAGCCUGGGGGCUCUCUGAGACUCUCCUGUGCAGCCUCUGGACUCGCCUUUAGUAUGUAUACCAUGGGCUGGUUCCGCCAGGCUCCAGGGAAGGAGCGUGAGUUUGUAGCAAUGAUUAUUUCAAGUGGUGAUAGCACCGACUACGCAGACUCCGUGAAGGGCCGAUUCACCAUCUCCAGGGACAACGGCAAGAACACGGUGUAUCUGCAAAUGGACAGCCUGAAACCUGAGGACACGGCCGUUUAUUACUGUGCAGCCCCAAAGUUUCGUUACUACUUUAGCACCUCUCCAGGUGAUUUUGAUUCCUGGGGCCAGGGGACCCAGGUCACCGUCUCCUCAGCGGCCGCAUACCCGUACGACGUUCCGGACUACGGUUCCCACCACCAUCACCAUCACUAGG.

The mRNA for tdTomato has the following sequence and includes a 5′-CAP and a poly-A tail: gagagccgccaccAUGGUGAGCAAGGGCGAGGAGGUCAUCAAAGAGUUCAUGCGCUUCAAGGUGCGC

AUGGAGGGCUCCAUGAACGGCCACGAGUUCGAGAUCGAG
GGCGAGGGCGAGGGCCGCCCCUACGAGGGCACCCAGACC
GCCAAGCUGAAGGUGACCAAGGGCGGCCCCCUGCCCUUC
GCCUGGGACAUCCUGUCCCCCCAGUUCAUGUACGGCUCC
AAGGCGUACGUGAAGCACCCCGCCGACAUCCCCGAUUAC
AAGAAGCUGUCCUUCCCCGAGGGCUUCAAGUGGGAGCGC
GUGAUGAACUUCGAGGACGGCGGUCUGGUGACCGUGACC
CAGGACUCCUCCCUGCAGGACGGCACGCUGAUCUACAAG
GUGAAGAUGCGCGGCACCAACUUCCCCCCCGACGGCCCC
GUAAUGCAGAAGAAGACCAUGGGCUGGGAGGCCUCCACC
GAGCGCCUGUACCCCCGCGACGGCGUGCUGAAGGGCGAG
AUCCACCAGGCCCUGAAGCUGAAGGACGGCGGCCACUAC
CUGGUGGAGUUCAAGACCAUCUACAUGGCCAAGAAGCCC
GUGCAACUGCCCGGCUACUACUACGUGGACACCAAGCUG
GACAUCACCUCCCACAACGAGGACUACACCAUCGUGGAA
CAGUACGAGCGCUCCGAGGGCCGCCACCACCUGUUCCUG
GGGCAUGGCACCGGCAGCACCGGCAGCGGCAGCUCCGGC
ACCGCCUCCUCCGAGGACAACAACAUGGCCGUCAUCAAA
GAGUUCAUGCGCUUCAAGGUGCGCAUGGAGGGCUCCAUG
AACGGCCACGAGUUCGAGAUCGAGGGCGAGGGCGAGGGC
CGCCCCUACGAGGGCACCCAGACCGCCAAGCUGAAGGUG
ACCAAGGGCGGCCCCCUGCCCUUCGCCUGGGACAUCCUG
UCCCCCCAGUUCAUGUACGGCUCCAAGGCGUACGUGAAG
CACCCCGCCGACAUCCCCGAUUACAAGAAGCUGUCCUUC
CCCGAGGGCUUCAAGUGGGAGCGCGUGAUGAACUUCGAG
GACGGCGGUCUGGUGACCGUGACCCAGGACUCCUCCCUG
CAGGACGGCACGCUGAUCUACAAGGUGAAGAUGCGCGGC
ACCAACUUCCCCCCCGACGGCCCCGUAAUGCAGAAGAAGA
CCAUGGGCUGGGAGGCCUCCACCGAGCGCCUGUACCCCC
GCGACGGCGUGCUGAAGGGCGAGAUCCACCAGGCCCUGA
AGCUGAAGGACGGCGGCCACUACCUGGUGGAGUUCAAGA
CCAUCUACAUGGCCAAGAAGCCCGUGCAACUGCCCGGCU
ACUACUACGUGGACACCAAGCUGGACAUCACCUCCCACA
ACGAGGACUACACCAUCGUGGAACAGUACGAGCGCUCCG
AGGGCCGCCACCACCUGUUCCUGUACGGCAUGGACGAGC
UGUACAAGUCCGGACUCAGAUCUAAGCUGAACCCUCCUG
AUGAGAGUGGCCCCGGCUGCAUGAGCUGCAAGUGUGUGC
UCUCCUGA.

LNP production

The LNP-mRNA was prepared using NanoAssemblr (Precision Nanosystems) microfluidic mixing technology under time-invariant conditions. 2 mL of an aqueous solution containing the mRNA at a concentration of 174 ng/μL in aqueous 70 mM acetate buffer, pH 4.0, was mixed with 1 mL aqueous ethanolic lipid solution containing 12.5 mM lipids to form the nanoparticles. The flow rate ratio between the aqueous solution and the aqueous ethanolic lipid solution was 3:1, and the total flow rate was 12 mL/min.

The aqueous ethanolic lipid solution was prepared by dissolving C12-200 (Corden Pharma), DOPE (1,2-dioleoyl-sn-glycero-3-phosphoethanolamine), cholesterol, DMG-PEG (PEGylated myristoyl diglyceride; Avanti catalog no. 880151P-1G) and DOTAP (1,2-di-(9Z-octadecenoyl)-3-trimethylammonium propane methylsulfate Avanti catalog no. 890890-200 mg) in a molar ratio of 29.8:13.6:39.5:2.1:15 in ethanol. This was done by preparing separate 12.5-mM solutions of each lipid in the ethanol and mixing the solutions in the ratio given above to give the aqueous ethanolic lipid solution.

We immediately diluted with 1.6 mL of the obtained LNP-mRNA product 64 mL PBS (1×) and concentrated to 1.5 mL at 2,000×*g* for 30 min at 20°C using Amicon Ultra-15 centrifugal filtration tubes. Finally, the LNP sample was sterilized with a 0.2-μm syringe filter and stored at 4°C.

Particle size was measured as the hydrodynamic diameter (intensity-averaged particle size, Z-average) with a ZetaSizer Ultra dynamic light scattering instrument from Malvern Panalytical. Samples were measured in triplicate through backscatter detection after production. Specifically, particle size was measured within the following instrument setting. The temperature was set at 25°C with the return to set default temperature after each measurement. Equilibration time was 10 s, data processing was set with automatic size display limit mode and general purpose analysis model. Regarding advanced settings options, data were collected in backscatter (angle of detection), with optimal positioning method, automatic attenuation, and measurement process. No pause after subruns and no optical filter was applied. Samples after microfluidics production were diluted 1:20 in PBS buffer placed in the cuvettes DTS0012. Results are given as *Z*-average diameter [nm].

The zeta potential was measured with a 100-fold LNP dilution in 800 μL PBS using the DTS1070 capillary cell. The size distribution of particles is 70.7 nm, particle number 5.31E+11, and zeta potential 0.51 mV.

mRNA delivery with LNPs

HEK 293T cells were plated in a complete medium at a density of 30000 cells and 100 μL per well in a 96-well plate (transparent flat bottom, Sarstedt) and incubated for 24 h in 5% CO_2 at 37°C. LNPs carrying mRNA for tdTomato (LNP-mRNA-tdTomato) or the nanobody (LNP-mRNA-2NSP23) were added to the cells at different dilutions and the cells were incubated overnight (16 h) at the 5% CO_2 37°C Incucyte incubator. Untreated HEK 293T cells were used as an autofluorescence control.

Analysis of tdTomato expression levels after LNP delivery by live-cell imaging

For monitoring tdTomato expression levels, cells were scanned for red signal detection during 16 h incubation with the different dilutions of LNP-mRNA-tdTomato. Live-cell imaging was done with an S3 Incucyte (S3/SX1 G/R Optical Module, Sartorius) for red and phase channels, acquisition time of 400 ms for both channels, and magnification of 10×. Total Red Object Integrated Intensity was quantified for each condition using the Incucyte Software Basic Analyzer. The analysis definitions used for the red signal were segmentation Top-Hat, radius 40 μm, and threshold 0.4 RCU with

Edge Split Off. A filter for a minimum of 20 μm^2 of area was used to remove debris from the analysis.

Analysis of nanobody expression levels after LNP delivery by immunostaining

After 16 h of incubation with the LNP-mRNA-2NSP23, cells were fixed by adding 100 μL 8% PFA for 20 min at room temperature (RT) (final concentration of PFA is 4%). All media were then gently removed and cells were washed three times for 5 min with 150 μL PBS. After the last wash, 100 μL of a blocking/permeabilization buffer (5% BSA and 0.2% Triton in PBS; BSA from Sigma; Triton X-100 from VWR) was added and cells were incubated for 1h at RT. Cells were then washed three times for 5 min with 150 μL PBS and staining was performed. For immunostaining, 50 μL of a 1:100 dilution of the AF488 goat anti-alpaca VHH secondary antibody was used (Jackson Immuno Research). For all cases, the antibody was prepared fresh at 1:100 in PBA (1% BSA in PBS). Incubation with the antibody was performed for 1 h at RT and protected from light. After nanobody staining cells were washed 3 times for 5 min with 150 μL PBS and then incubated for 5 min with 100 μL of DAPI 1:1000 in PBS for nuclear staining (DAPI from Sigma). The last three washes were then performed and cells were imaged directly at the 96-well plate with an inverted DMi8 microscope (Leica). For image acquisition, the same exposure times were used for each corresponding channel, between the different conditions.

SARS-CoV-2 infection assays

Viruses used in this study are recombinant infectious strains icSARS-CoV-2-mNeonGreen[36] and icSARS-CoV-2-nLuc,[38] and wild-type viruses Wuhan strain (Hu-1), UK variant or B1.617X (Alpha), B1.621 (Mu), B1.617.x (Delta), and B1.1.529 (Omicron), which were isolated at REGA Institute (Katholieke Universiteit Leuven, Belgium) in 2021.[66–69] In all experiments, viruses were used at 0.1 of multiplicity of infection (MOI). 2×10^5 Vero E6 cells, HEK293-ACE2, or Huh7.5 cells were cultured in 24-well plates in DMEM (Sigma D5796) containing 10% of fetal bovine serum, 2 mM of L-glutamine, 100 U penicillin, and 100 g/L of streptomycin in a cell culture incubator at 37° with 5% CO_2 and 95% humidity. After 24 h, cells were treated with an increased concentration of LNP-encapsulated mRNA molecules encoding for the nanobody 2NSP23 targeting NSP9 protein or mRNA molecules encoding tdTomato, as a control. The mRNAs were encapsulated in LNPs, with initial working concentrations of mRNA of 200 ng/μL, and five serial dilutions of 2-fold were used. After 8 h of incubation, cells were infected with indicated strains of SARS-CoV-2 at 0.1 of MOI. The next day, after 16 h of culture, cells were either lysed for RNA extraction, nano-luciferase quantified in the case of icSARS-CoV-2-nLuc, or fixed with 3.7% paraformaldehyde during 20 min followed by fluorescent analysis using Incucyte S3 instrument. For the icSARS-CoV-2-mNeonGreen replication efficiency, fluorescence quantification was performed using Incucyte software, and EC_{50} values were calculated via the variable slope model in GraphPad Prism v8. For the icSARS-CoV-2-nLuc, luminescence was quantified using Molecular Devices Instrument. Cell viability was measured using the Cell Titer-Glo Luminescent Cell Viability Assay kit (Promega, G7750). Nano-luminescence values were normalized with corresponding viability data to control for any inherent toxicity of LNP-mRNA formulations.[39]

RNA extraction and RT-qPCR

HEK293-ACE2 cells were infected as above with different strains of SARS-CoV-2 - original Wuhan strain (Hu-1), UK variant or B1.617X (Alpha), B1.621 (Mu), B1.617.x (Delta), and B1.1.529 (Omicron), and treated with LNP-mRNA (0.4 ng/μL) complexes encoding either the nanobody NSP23 targeting NSP9 (LNP-mRNA-2NSP23) or mRNA molecules encoding tdTomato (LNP-mRNA-tdTomato), as a control. Twenty-four hours post-infection (pi), cells were washed with PBS and lysed with RNA extraction buffer (Nucleo spin RNA extraction kit, Macherey-Nagel, Cat# 740955). Total RNA was extracted according to the manufacturer's instructions, concentrations were determined using Nanodrop (Thermo), and the integrity of RNA was verified using Agilent 2100 Bioanalyser Systems. One nanogram of RNA was subsequently used in a one-step RT-qPCR for the E gene of SARS-CoV-2 using the following primers: F: 5′- ACAG GTACGTTAATAGTTAATAGCGT-3′ and R: 5′-ATATTGCAG CAGTACGCACACA-3′ for amplification, and the double dye probe P: 5'-(FAM) ACACTAGCCATCCTTACTGCGCTTCG (BHQ)-3′ as previously described.[70]

RNA-seq analysis

HEK293-ACE2 cells either infected with the SARS-CoV-2 virus (named by variant) or uninfected (NC), treated with LNPs containing mRNA sequences of either the anti-NSP9 nanobody (NSP) or tdTomato (Tom) were used for total mRNA isolation by TRI Reagent (Millipore-Sigma) according to the manufacturer's protocol. Three biological replicates for each condition were used for transcriptional profiling. The RNA-Seq library was prepared by using the NEBNext Ultra II RNA Library Prep Kit for Illumina (NEB) and sequenced with the NextSeq 500/550 sequencing platform (performed at the NYUAD Sequencing Center). Raw FASTQ sequenced reads were first assessed for quality using FastQC v0.11.5 (https://www.bioinformatics.babraham.ac.uk/projects/fastqc/). The reads were then passed through Trimmomatic v0.36 for quality trimming and adapter sequence removal, with the parameters (ILLUMINACLIP: trimmomatic_adapter.fa:2:30:10 TRAILING:3 LEADING:3 SLIDINGWINDOW:4:15 MINLEN:36).[71] The surviving trimmed read pairs were then processed with Fastp to remove poly-G tails and Novaseq/Nextseq-specific artifacts.[72] Following the quality trimming, the reads were assessed again using FastQC.

Post QC and QT, the reads were aligned to the human reference genome GRCh38.81 using HISAT2[73] with the default parameters and additionally by providing the –dta flag. The resulting SAM alignments were then converted to BAM, while retaining only the unmapped read pairs using SAMtools[74] v1.9 "samtools view -f 12 -F 256 -b INPUT.sam > OUTPUT.bam." The resulting unmapped BAM reads were then sorted and converted to fastq reads using samtools sort "samtools sort -@ 14 -o OUTPUT.sorted.bam INPUT.bam" and samtools fastq "samtools fastq −1 read1.fastq −2 read2.fastq -@ 14 INPUT.sorted.bam." These unmapped reads were then aligned to

the SARS-COV-2 reference genome available through NCBI with the accession NC_045512.2 using HISAT2 with the same parameters that were used in the initial mapping to the human reference. The resulting SAM alignments were then converted to BAM format and coordinate sorted using samtools view and samtools sort, respectively. Read groups were then added to the sorted SARS-COV-2 mapped BAM files using Picard AddOrReplaceReadGroups (http://broadinstitute.github.io/picard/). A consensus genome was then generated for each SARS-COV-2 sample using samtools mpileup and ivar[75] version 1.3 with the minimum depth set at 20 "samtools mpileup -A -d 0 -Q 0 INPUT.sorted.bam | ivar consensus -m 20 -p OUTPUT.sars-cov-2-consensus.fasta." Finally, Qualimap[76] v2.2.2 was used to generate alignment-specific QC metrics per sample, both for alignments vs. the human reference, as well as the SARS-COV-2 reference. The BAM alignment files were processed using HTseq-count, using the reference annotation file to produce raw counts for each sample. The raw counts were then analyzed using the online analysis portal NASQAR (http://nasqar.abudhabi.nyu.edu/), to merge, normalize, and identify DEGs. DEGs (log2(FC) $\geq$ 0.5 and adjusted p value of < 0.05 for up-regulated genes, and log2(FC) ≤ -0.5 and adjusted p value of < 0.05 for down-regulated genes) between each sample combination were subjected to GO enrichment using DAVID Bioinformatics (https://david.ncifcrf.gov/).[77] The full RNA-Seq dataset was deposited in the Gene Expression Omnibus (GEO) database under accession number GSE244714 (Gene Expression Omnibus: GSE244714).

Viral infection of human 3D reconstituted human upper airway epithelium tissues and subsequent quantification

The 3D reconstituted human upper airway epithelium tissues from healthy donors were provided by Epithelix company and maintained in an ALI in Costar Transwell insert (Corning). On day 0 of the experiment, the 3D reconstituted epithelium was pre-treated for 24 h with basal medium containing LNP-mRNA-2NSP23 or LNP-mRNA-tdTomato, followed by incubation with SARS-CoV-2 at 1 $\times$ 10^3 TCID50/insert virus (150 µL) input at the apical side for 1 h and subsequent removal of the inoculum. A first apical wash with OptiMEM media was performed on day 1 pi, but this was not retained for analysis. On day 2, the medium at the basolateral side of the 3D reconstituted epithelium was replaced with fresh medium, and on day 2 (48 h pi) and day 4 (96 h pi), apical washes were collected for viral quantification.

Viral RNA from apical wash was extracted using QIAamp Viral RNA Kits (QIAGEN), and quantified using one-step RT-qPCR for the E gene of SARS-CoV-2 using the following primers: F: 5′- ACAGGTA CGTTAATAGTTAATAGCGT-3′ and R: 5′-ATATTGCAGCAGT ACGCACACA-3′ for amplification, and the double dye probe P1 5'-(FAM) ACACTAGCCATCCTTACTGCGCTTCG (BHQ)-3′ for quantification. Changes in gene expression were calculated using the $2^{-\Delta Ct}$ method.

DATA AND CODE AVAILABILITY

Gene expression data are publicly available in the Gene Expression Omnibus: GSE244714.

ACKNOWLEDGMENTS

This work is supported by grants from NYU Abu Dhabi, the Sheikh Hamdan Bin Rashid Al Maktoum Award for Medical Sciences, a donation from the Cipriani family, a COVID-19 Facilitator Grant from NYU Abu Dhabi and Tamkeen under the NYU Abu Dhabi Research Institute Award to the NYUAD Center for Genomics and Systems Biology (ADHPG-CGSB) to P.P.; a Fonds de la Recherche Scientifique (FRS-FNRS) PER Coronavirus grant 40003579 to J.-C.T. and Télevie grant 40002377 to J.-C.T. and J.B., an FRS-FNRS postdoctoral grant 40011260 to S.M.; and a Foundation Léon Fredericq (FLF) grant to J.B. We thank the NYU Abu Dhabi Center for Genomics and Systems Biology, in particular Marc Arnoux and Mehar Sultana for RNA sequencing. We thank the ULIEGE-GIGA Institute Viral Vectors and Cell Imaging for Biosafety Laboratory Level 3 (BSL3) and imaging systems access, respectively. We appreciate the computational platform provided by the Center for Genomics and Systems Biology and the NYU Abu Dhabi HPC team and are especially thankful to Nizar Drou for technical help.

AUTHOR CONTRIBUTIONS

P.P. conceived the research and wrote the manuscript with T.V. T.V. and S.S. performed all RNA-seq analyses, and data analysis and prepared the corresponding figures. J.C.T., J.B., and S.B.M. performed functional assays and L.E. and C.B. performed the imaging. H.P.H. and S.D. performed LNP characterization. P.P., J.C.T., T.V., M.L., and G.E. analyzed the results. P.P. supervised all the research. All authors read and approved the manuscript.

DECLARATION OF INTERESTS

P.P., G.E., H.T.H., and S.C.D. are part of a US patent filed by New York University in Abu Dhabi jointly with ISAR Biosciences.

SUPPLEMENTAL INFORMATION

Supplemental information can be found online at https://doi.org/10.1016/j.omtn.2024.102304.

REFERENCES

1. Hamre, D., and Procknow, J.J. (1966). A new virus isolated from the human respiratory tract. Proc. Soc. Exp. Biol. Med. *121*, 190–193. https://doi.org/10.3181/00379727-121-30734.
2. McIntosh, K., Kapikian, A.Z., Turner, H.C., Hartley, J.W., Parrott, R.H., and Chanock, R.M. (1970). Seroepidemiologic studies of coronavirus infection in adults and children. Am. J. Epidemiol. *91*, 585–592. https://doi.org/10.1093/oxfordjournals.aje.a121171.
3. van der Hoek, L., Pyrc, K., Jebbink, M.F., Vermeulen-Oost, W., Berkhout, R.J.M., Wolthers, K.C., Wertheim-van Dillen, P.M.E., Kaandorp, J., Spaargaren, J., and Berkhout, B. (2004). Identification of a new human coronavirus. Nat. Med. *10*, 368–373. https://doi.org/10.1038/nm1024.
4. Woo, P.C.Y., Lau, S.K.P., Chu, C.M., Chan, K.H., Tsoi, H.W., Huang, Y., Wong, B.H.L., Poon, R.W.S., Cai, J.J., Luk, W.K., et al. (2005). Characterization and complete genome sequence of a novel coronavirus, coronavirus HKU1, from patients with pneumonia. J. Virol. *79*, 884–895. https://doi.org/10.1128/JVI.79.2.884-895.2005.
5. Matoba, Y., Abiko, C., Ikeda, T., Aoki, Y., Suzuki, Y., Yahagi, K., Matsuzaki, Y., Itagaki, T., Katsushima, F., Katsushima, Y., and Mizuta, K. (2015). Detection of the human coronavirus 229E, HKU1, NL63, and OC43 between 2010 and 2013 in Yamagata, Japan. Jpn. J. Infect. Dis. *68*, 138–141. https://doi.org/10.7883/yoken.JJID.2014.266.
6. Otieno, J.R., Cherry, J.L., Spiro, D.J., Nelson, M.I., and Trovão, N.S. (2022). Origins and Evolution of Seasonal Human Coronaviruses. Viruses *14*, 1551. https://doi.org/10.3390/v14071551.
7. Zhong, N.S., Zheng, B.J., Li, Y.M., Xie, Z.H., Chan, K.H., Li, P.H., Tan, S.Y., Chang, Q., Xie, J.P., Liu, X.Q., et al. (2003). Epidemiology and cause of severe acute respiratory syndrome (SARS) in Guangdong, People's Republic of China, in February, 2003. Lancet *362*, 1353–1358. https://doi.org/10.1016/s0140-6736(03)14630-2.
8. Wang, D., Hu, B., Hu, C., Zhu, F., Liu, X., Zhang, J., Wang, B., Xiang, H., Cheng, Z., Xiong, Y., et al. (2020). Clinical Characteristics of 138 Hospitalized Patients With 2019 Novel Coronavirus-Infected Pneumonia in Wuhan, China. JAMA *323*, 1061–1069. https://doi.org/10.1001/jama.2020.1585.

9. V'Kovski, P., Kratzel, A., Steiner, S., Stalder, H., and Thiel, V. (2021). Coronavirus biology and replication: implications for SARS-CoV-2. Nat. Rev. Microbiol. *19*, 155–170. https://doi.org/10.1038/s41579-020-00468-6.

10. Brian, D.A., and Baric, R.S. (2005). Coronavirus genome structure and replication. Curr. Top. Microbiol. Immunol. *287*, 1–30. https://doi.org/10.1007/3-540-26765-4_1.

11. Woo, P.C.Y., Huang, Y., Lau, S.K.P., and Yuen, K.Y. (2010). Coronavirus genomics and bioinformatics analysis. Viruses *2*, 1804–1820. https://doi.org/10.3390/v2081803.

12. Fehr, A.R., and Perlman, S. (2015). Coronaviruses: an overview of their replication and pathogenesis. Methods Mol. Biol. *1282*, 1–23. https://doi.org/10.1007/978-1-4939-2438-7_1.

13. Yan, L., Zhang, Y., Ge, J., Zheng, L., Gao, Y., Wang, T., Jia, Z., Wang, H., Huang, Y., Li, M., et al. (2020). Architecture of a SARS-CoV-2 mini replication and transcription complex. Nat. Commun. *11*, 5874. https://doi.org/10.1038/s41467-020-19770-1.

14. Esposito, G., Hunashal, Y., Percipalle, M., Fogolari, F., Venit, T., Leonchiks, A., Gunsalus, K.C., Piano, F., and Percipalle, P. (2024). Assessing nanobody interaction with SARS-CoV-2 Nsp9. PLoS One *19*, e0303839. https://doi.org/10.1371/journal.pone.0303839.

15. Esposito, G., Hunashal, Y., Percipalle, M., Venit, T., Dieng, M.M., Fogolari, F., Hassanzadeh, G., Piano, F., Gunsalus, K.C., Idaghdour, Y., and Percipalle, P. (2021). NMR-Based Analysis of Nanobodies to SARS-CoV-2 Nsp9 Reveals a Possible Antiviral Strategy Against COVID-19. Adv. Biol. *5*, e2101113. https://doi.org/10.1002/adbi.202101113.

16. Ponnusamy, R., Moll, R., Weimar, T., Mesters, J.R., and Hilgenfeld, R. (2008). Variable oligomerization modes in coronavirus non-structural protein 9. J. Mol. Biol. *383*, 1081–1096. https://doi.org/10.1016/j.jmb.2008.07.071.

17. Zhang, C., Chen, Y., Li, L., Yang, Y., He, J., Chen, C., and Su, D. (2020). Structural basis for the multimerization of nonstructural protein nsp9 from SARS-CoV-2. Mol. Biomed. *1*, 5. https://doi.org/10.1186/s43556-020-00005-0.

18. Yan, L., Ge, J., Zheng, L., Zhang, Y., Gao, Y., Wang, T., Huang, Y., Yang, Y., Gao, S., Li, M., et al. (2021). Cryo-EM Structure of an Extended SARS-CoV-2 Replication and Transcription Complex Reveals an Intermediate State in Cap Synthesis. Cell *184*, 184–193.e10. https://doi.org/10.1016/j.cell.2020.11.016.

19. Sutton, G., Fry, E., Carter, L., Sainsbury, S., Walter, T., Nettleship, J., Berrow, N., Owens, R., Gilbert, R., Davidson, A., et al. (2004). The nsp9 replicase protein of SARS-coronavirus, structure and functional insights. Structure *12*, 341–353. https://doi.org/10.1016/j.str.2004.01.016.

20. Miknis, Z.J., Donaldson, E.F., Umland, T.C., Rimmer, R.A., Baric, R.S., and Schultz, L.W. (2009). Severe acute respiratory syndrome coronavirus nsp9 dimerization is essential for efficient viral growth. J. Virol. *83*, 3007–3018. https://doi.org/10.1128/JVI.01505-08.

21. Zeng, Z., Deng, F., Shi, K., Ye, G., Wang, G., Fang, L., Xiao, S., Fu, Z., and Peng, G. (2018). Dimerization of Coronavirus nsp9 with Diverse Modes Enhances Its Nucleic Acid Binding Affinity. J. Virol. *92*, e00692-18. https://doi.org/10.1128/JVI.00692-18.

22. Egloff, M.P., Ferron, F., Campanacci, V., Longhi, S., Rancurel, C., Dutartre, H., Snijder, E.J., Gorbalenya, A.E., Cambillau, C., and Canard, B. (2004). The severe acute respiratory syndrome-coronavirus replicative protein nsp9 is a single-stranded RNA-binding subunit unique in the RNA virus world. Proc. Natl. Acad. Sci. USA *101*, 3792–3796. https://doi.org/10.1073/pnas.0307877101.

23. Littler, D.R., Gully, B.S., Colson, R.N., and Rossjohn, J. (2020). Crystal Structure of the SARS-CoV-2 Non-structural Protein 9, Nsp9. iScience *23*, 101258. https://doi.org/10.1016/j.isci.2020.101258.

24. Dong, J., Huang, B., Jia, Z., Wang, B., Gallolu Kankanamalage, S., Titong, A., and Liu, Y. (2020). Development of multi-specific humanized llama antibodies blocking SARS-CoV-2/ACE2 interaction with high affinity and avidity. Emerg. Microb. Infect. *9*, 1034–1036. https://doi.org/10.1080/22221751.2020.1768806.

25. Huo, J., Le Bas, A., Ruza, R.R., Duyvesteyn, H.M.E., Mikolajek, H., Malinauskas, T., Tan, T.K., Rijal, P., Dumoux, M., Ward, P.N., et al. (2020). Neutralizing nanobodies bind SARS-CoV-2 spike RBD and block interaction with ACE2. Nat. Struct. Mol. Biol. *27*, 846–854. https://doi.org/10.1038/s41594-020-0469-6.

26. Ma, H., Zhang, X., Zheng, P., Dube, P.H., Zeng, W., Chen, S., Cheng, Q., Yang, Y., Wu, Y., Zhou, J., et al. (2022). Hetero-bivalent nanobodies provide broad-spectrum protection against SARS-CoV-2 variants of concern including Omicron. Cell Res. *32*, 831–842. https://doi.org/10.1038/s41422-022-00700-3.

27. Maeda, R., Fujita, J., Konishi, Y., Kazuma, Y., Yamazaki, H., Anzai, I., Watanabe, T., Yamaguchi, K., Kasai, K., Nagata, K., et al. (2022). A panel of nanobodies recognizing conserved hidden clefts of all SARS-CoV-2 spike variants including Omicron. Commun. Biol. *5*, 669. https://doi.org/10.1038/s42003-022-03630-3.

28. Wrapp, D., De Vlieger, D., Corbett, K.S., Torres, G.M., Wang, N., Van Breedam, W., Roose, K., van Schie, L.; VIB-CMB COVID-19 Response Team, and Hoffmann, M., et al. (2020). Structural Basis for Potent Neutralization of Betacoronaviruses by Single-Domain Camelid Antibodies. Cell *181*, 1004–1015.e15. https://doi.org/10.1016/j.cell.2020.04.031.

29. Plessner, M., Melak, M., Chinchilla, P., Baarlink, C., and Grosse, R. (2015). Nuclear F-actin formation and reorganization upon cell spreading. J. Biol. Chem. *290*, 11209–11216. https://doi.org/10.1074/jbc.M114.627166.

30. Schiavon, C.R., Zhang, T., Zhao, B., Moore, A.S., Wales, P., Andrade, L.R., Wu, M., Sung, T.C., Dayn, Y., Feng, J.W., et al. (2020). Actin chromobody imaging reveals sub-organellar actin dynamics. Nat. Methods *17*, 917–921. https://doi.org/10.1038/s41592-020-0926-5.

31. Semple, S.C., Akinc, A., Chen, J., Sandhu, A.P., Mui, B.L., Cho, C.K., Sah, D.W.Y., Stebbing, D., Crosley, E.J., Yaworski, E., et al. (2010). Rational design of cationic lipids for siRNA delivery. Nat. Biotechnol. *28*, 172–176. https://doi.org/10.1038/nbt.1602.

32. Maurer, N., Wong, K.F., Stark, H., Louie, L., McIntosh, D., Wong, T., Scherrer, P., Semple, S.C., and Cullis, P.R. (2001). Spontaneous entrapment of polynucleotides upon electrostatic interaction with ethanol-destabilized cationic liposomes. Biophys. J. *80*, 2310–2326. https://doi.org/10.1016/S0006-3495(01)76202-9.

33. Corbett, K.S., Edwards, D.K., Leist, S.R., Abiona, O.M., Boyoglu-Barnum, S., Gillespie, R.A., Himansu, S., Schäfer, A., Ziwawo, C.T., DiPiazza, A.T., et al. (2020). SARS-CoV-2 mRNA vaccine design enabled by prototype pathogen preparedness. Nature *586*, 567–571. https://doi.org/10.1038/s41586-020-2622-0.

34. Hassett, K.J., Benenato, K.E., Jacquinet, E., Lee, A., Woods, A., Yuzhakov, O., Himansu, S., Deterling, J., Geilich, B.M., Ketova, T., et al. (2019). Optimization of Lipid Nanoparticles for Intramuscular Administration of mRNA Vaccines. Mol. Ther. Nucleic Acids *15*, 1–11. https://doi.org/10.1016/j.omtn.2019.01.013.

35. Wei, W., Sun, J., Guo, X.Y., Chen, X., Wang, R., Qiu, C., Zhang, H.T., Pang, W.H., Wang, J.C., and Zhang, Q. (2020). Microfluidic-Based Holonomic Constraints of siRNA in the Kernel of Lipid/Polymer Hybrid Nanoassemblies for Improving Stable and Safe In Vivo Delivery. ACS Appl. Mater. Interfaces *12*, 14839–14854. https://doi.org/10.1021/acsami.9b22781.

36. Xie, X., Muruato, A., Lokugamage, K.G., Narayanan, K., Zhang, X., Zou, J., Liu, J., Schindewolf, C., Bopp, N.E., Aguilar, P.V., et al. (2020). An Infectious cDNA Clone of SARS-CoV-2. Cell Host Microbe *27*, 841–848.e3. https://doi.org/10.1016/j.chom.2020.04.004.

37. Kim, D.K., Weller, B., Lin, C.W., Sheykhkarimli, D., Knapp, J.J., Dugied, G., Zanzoni, A., Pons, C., Tofaute, M.J., Maseko, S.B., et al. (2023). A proteome-scale map of the SARS-CoV-2-human contactome. Nat. Biotechnol. *41*, 140–149. https://doi.org/10.1038/s41587-022-01475-z.

38. Hou, Y.J., Okuda, K., Edwards, C.E., Martinez, D.R., Asakura, T., Dinnon, K.H., 3rd, Kato, T., Lee, R.E., Yount, B.L., Mascenik, T.M., et al. (2020). SARS-CoV-2 Reverse Genetics Reveals a Variable Infection Gradient in the Respiratory Tract. Cell *182*, 429–446.e14. https://doi.org/10.1016/j.cell.2020.05.042.

39. Bitounis, D., Jacquinet, E., Rogers, M.A., and Amiji, M.M. (2024). Strategies to reduce the risks of mRNA drug and vaccine toxicity. Nat. Rev. Drug Discov. *23*, 281–300. https://doi.org/10.1038/s41573-023-00859-3.

40. Zaffagni, M., Harris, J.M., Patop, I.L., Pamudurti, N.R., Nguyen, S., and Kadener, S. (2022). SARS-CoV-2 Nsp14 mediates the effects of viral infection on the host cell transcriptome. Elife *11*, e71945. https://doi.org/10.7554/eLife.71945.

41. Blanco-Melo, D., Nilsson-Payant, B.E., Liu, W.C., Uhl, S., Hoagland, D., Møller, R., Jordan, T.X., Oishi, K., Panis, M., Sachs, D., et al. (2020). Imbalanced Host Response to SARS-CoV-2 Drives Development of COVID-19. Cell *181*, 1036–1045.e9. https://doi.org/10.1016/j.cell.2020.04.026.

42. Chakraborty, D., Agrawal, A., and Maiti, S. (2021). Rapid identification and tracking of SARS-CoV-2 variants of concern. Lancet *397*, 1346–1347. https://doi.org/10.1016/S0140-6736(21)00470-0.

43. Sun, L., Li, P., Ju, X., Rao, J., Huang, W., Ren, L., Zhang, S., Xiong, T., Xu, K., Zhou, X., et al. (2021). In vivo structural characterization of the SARS-CoV-2 RNA genome identifies host proteins vulnerable to repurposed drugs. Cell *184*, 1865–1883.e20. https://doi.org/10.1016/j.cell.2021.02.008.

44. Wyler, E., Mösbauer, K., Franke, V., Diag, A., Gottula, L.T., Arsiè, R., Klironomos, F., Koppstein, D., Hönzke, K., Ayoub, S., et al. (2021). Transcriptomic profiling of SARS-CoV-2 infected human cell lines identifies HSP90 as target for COVID-19 therapy. iScience *24*, 102151. https://doi.org/10.1016/j.isci.2021.102151.

45. Bhowal, C., Ghosh, S., Ghatak, D., and De, R. (2023). Pathophysiological involvement of host mitochondria in SARS-CoV-2 infection that causes COVID-19: a comprehensive evidential insight. Mol. Cell. Biochem. *478*, 1325–1343. https://doi.org/10.1007/s11010-022-04593-z.

46. Gatti, P., Ilamathi, H.S., Todkar, K., and Germain, M. (2020). Mitochondria Targeted Viral Replication and Survival Strategies-Prospective on SARS-CoV-2. Front. Pharmacol. *11*, 578599. https://doi.org/10.3389/fphar.2020.578599.

47. Shang, C., Liu, Z., Zhu, Y., Lu, J., Ge, C., Zhang, C., Li, N., Jin, N., Li, Y., Tian, M., and Li, X. (2021). SARS-CoV-2 Causes Mitochondrial Dysfunction and Mitophagy Impairment. Front. Microbiol. *12*, 780768. https://doi.org/10.3389/fmicb.2021.780768.

48. Singh, K.K., Chaubey, G., Chen, J.Y., and Suravajhala, P. (2020). Decoding SARS-CoV-2 hijacking of host mitochondria in COVID-19 pathogenesis. Am. J. Physiol. Cell Physiol. *319*, C258–C267. https://doi.org/10.1152/ajpcell.00224.2020.

49. Zhao, X., Chen, D., Li, X., Griffith, L., Chang, J., An, P., and Guo, J.T. (2022). Interferon Control of Human Coronavirus Infection and Viral Evasion: Mechanistic Insights and Implications for Antiviral Drug and Vaccine Development. J. Mol. Biol. *434*, 167438. https://doi.org/10.1016/j.jmb.2021.167438.

50. Pizzorno, A., Padey, B., Julien, T., Trouillet-Assant, S., Traversier, A., Errazuriz-Cerda, E., Fouret, J., Dubois, J., Gaymard, A., Lescure, F.X., et al. (2020). Characterization and Treatment of SARS-CoV-2 in Nasal and Bronchial Human Airway Epithelia. Cell Rep. Med. *1*, 100059. https://doi.org/10.1016/j.xcrm.2020.100059.

51. Robinot, R., Hubert, M., de Melo, G.D., Lazarini, F., Bruel, T., Smith, N., Levallois, S., Larrous, F., Fernandes, J., Gellenoncourt, S., et al. (2021). SARS-CoV-2 infection induces the dedifferentiation of multiciliated cells and impairs mucociliary clearance. Nat. Commun. *12*, 4354. https://doi.org/10.1038/s41467-021-24521-x.

52. Jonsdottir, H.R., Siegrist, D., Julien, T., Padey, B., Bouveret, M., Terrier, O., Pizzorno, A., Huang, S., Samby, K., Wells, T.N.C., et al. (2022). Molnupiravir combined with different repurposed drugs further inhibits SARS-CoV-2 infection in human nasal epithelium *in vitro*. Biomed. Pharmacother. *150*, 113058. https://doi.org/10.1016/j.biopha.2022.113058.

53. Pinto, A.L., Rai, R.K., Brown, J.C., Griffin, P., Edgar, J.R., Shah, A., Singanayagam, A., Hogg, C., Barclay, W.S., Futter, C.E., and Burgoyne, T. (2022). Ultrastructural insight into SARS-CoV-2 entry and budding in human airway epithelium. Nat. Commun. *13*, 1609. https://doi.org/10.1038/s41467-022-29255-y.

54. Burtscher, J., Cappellano, G., Omori, A., Koshiba, T., and Millet, G.P. (2020). Mitochondria: In the Cross Fire of SARS-CoV-2 and Immunity. iScience *23*, 101631. https://doi.org/10.1016/j.isci.2020.101631.

55. Makiyama, K., Hazawa, M., Kobayashi, A., Lim, K., Voon, D.C., and Wong, R.W. (2022). NSP9 of SARS-CoV-2 attenuates nuclear transport by hampering nucleoporin 62 dynamics and functions in host cells. Biochem. Biophys. Res. Commun. *586*, 137–142. https://doi.org/10.1016/j.bbrc.2021.11.046.

56. Abbasian, M.H., Mahmanzar, M., Rahimian, K., Mahdavi, B., Tokhanbigli, S., Moradi, B., Sisakht, M.M., and Deng, Y. (2023). Global landscape of SARS-CoV-2 mutations and conserved regions. J. Transl. Med. *21*, 152. https://doi.org/10.1186/s12967-023-03996-w.

57. Ackaert, C., Smiejkowska, N., Xavier, C., Sterckx, Y.G.J., Denies, S., Stijlemans, B., Elkrim, Y., Devoogdt, N., Caveliers, V., Lahoutte, T., et al. (2021). Immunogenicity Risk Profile of Nanobodies. Front. Immunol. *12*, 632687. https://doi.org/10.3389/fimmu.2021.632687.

58. Bao, G., Tang, M., Zhao, J., and Zhu, X. (2021). Nanobody: a promising toolkit for molecular imaging and disease therapy. EJNMMI Res. *11*, 6. https://doi.org/10.1186/s13550-021-00750-5.

59. Lokugamage, M.P., Vanover, D., Beyersdorf, J., Hatit, M.Z.C., Rotolo, L., Echeverri, E.S., Peck, H.E., Ni, H., Yoon, J.K., Kim, Y., et al. (2021). Optimization of lipid nanoparticles for the delivery of nebulized therapeutic mRNA to the lungs. Nat. Biomed. Eng. *5*, 1059–1068. https://doi.org/10.1038/s41551-021-00786-x.

60. Kim, J., Jozic, A., Lin, Y., Eygeris, Y., Bloom, E., Tan, X., Acosta, C., MacDonald, K.D., Welsher, K.D., and Sahay, G. (2022). Engineering Lipid Nanoparticles for Enhanced Intracellular Delivery of mRNA through Inhalation. ACS Nano *16*, 14792–14806. https://doi.org/10.1021/acsnano.2c05647.

61. Leong, E.W.X., and Ge, R. (2022). Lipid Nanoparticles as Delivery Vehicles for Inhaled Therapeutics. Biomedicines *10*, 2179. https://doi.org/10.3390/biomedicines10092179.

62. Li, B., Manan, R.S., Liang, S.Q., Gordon, A., Jiang, A., Varley, A., Gao, G., Langer, R., Xue, W., and Anderson, D. (2023). Combinatorial design of nanoparticles for pulmonary mRNA delivery and genome editing. Nat. Biotechnol. *41*, 1410–1415. https://doi.org/10.1038/s41587-023-01679-x.

63. Van Heeke, G., Allosery, K., De Brabandere, V., De Smedt, T., Detalle, L., and de Fougerolles, A. (2017). Nanobodies(R) as inhaled biotherapeutics for lung diseases. Pharmacol. Ther. *169*, 47–56. https://doi.org/10.1016/j.pharmthera.2016.06.012.

64. Kon, E., Elia, U., and Peer, D. (2022). Principles for designing an optimal mRNA lipid nanoparticle vaccine. Curr. Opin. Biotechnol. *73*, 329–336. https://doi.org/10.1016/j.copbio.2021.09.016.

65. Small, G.I., Fedorova, O., Olinares, P.D.B., Chandanani, J., Banerjee, A., Choi, Y.J., Molina, H., Chait, B.T., Darst, S.A., and Campbell, E.A. (2023). Structural and functional insights into the enzymatic plasticity of the SARS-CoV-2 NiRAN domain. Mol. Cell *83*, 3921–3930.e7. https://doi.org/10.1016/j.molcel.2023.10.001.

66. Dellicour, S., Durkin, K., Hong, S.L., Vanmechelen, B., Martí-Carreras, J., Gill, M.S., Meex, C., Bontems, S., André, E., Gilbert, M., et al. (2021). A Phylodynamic Workflow to Rapidly Gain Insights into the Dispersal History and Dynamics of SARS-CoV-2 Lineages. Mol. Biol. Evol. *38*, 1608–1613. https://doi.org/10.1093/molbev/msaa284.

67. Baggen, J., Persoons, L., Vanstreels, E., Jansen, S., Van Looveren, D., Boeckx, B., Geudens, V., De Man, J., Jochmans, D., Wauters, J., et al. (2021). Genome-wide CRISPR screening identifies TMEM106B as a proviral host factor for SARS-CoV-2. Nat. Genet. *53*, 435–444. https://doi.org/10.1038/s41588-021-00805-2.

68. Sharma, S., Vercruysse, T., Sanchez-Felipe, L., Kerstens, W., Rasulova, M., Bervoets, L., De Keyzer, C., Abdelnabi, R., Foo, C.S., Lemmens, V., et al. (2022). Updated vaccine protects against SARS-CoV-2 variants including Omicron (B.1.1.529) and prevents transmission in hamsters. Nat. Commun. *13*, 6644. https://doi.org/10.1038/s41467-022-34439-7.

69. Bruel, T., Stéfic, K., Nguyen, Y., Toniutti, D., Staropoli, I., Porrot, F., Guivel-Benhassine, F., Bolland, W.H., Planas, D., Hadjadj, J., et al. (2022). Longitudinal analysis of serum neutralization of SARS-CoV-2 Omicron BA.2, BA.4, and BA.5 in patients receiving monoclonal antibodies. Cell Rep. Med. *3*, 100850. https://doi.org/10.1016/j.xcrm.2022.100850.

70. Coupeau, D., Burton, N., Lejeune, N., Loret, S., Petit, A., Pejakovic, S., Poulain, F., Bonil, L., Trozzi, G., Wiggers, L., et al. (2020). SARS-CoV-2 Detection for Diagnosis Purposes in the Setting of a Molecular Biology Research Lab. Methods Protoc. *3*, 59. https://doi.org/10.3390/mps3030059.

71. Bolger, A.M., Lohse, M., and Usadel, B. (2014). Trimmomatic: a flexible trimmer for Illumina sequence data. Bioinformatics *30*, 2114–2120. https://doi.org/10.1093/bioinformatics/btu170.

72. Chen, S., Zhou, Y., Chen, Y., and Gu, J. (2018). fastp: an ultra-fast all-in-one FASTQ preprocessor. Bioinformatics *34*, i884–i890. https://doi.org/10.1093/bioinformatics/bty560.

73. Kim, D., Langmead, B., and Salzberg, S.L. (2015). HISAT: a fast spliced aligner with low memory requirements. Nat. Methods *12*, 357–360. https://doi.org/10.1038/nmeth.3317.

74. Li, H., Handsaker, B., Wysoker, A., Fennell, T., Ruan, J., Homer, N., Marth, G., Abecasis, G., and Durbin, R.; 1000 Genome Project Data Processing Subgroup

(2009). The Sequence Alignment/Map format and SAMtools. Bioinformatics *25*, 2078–2079. https://doi.org/10.1093/bioinformatics/btp352.

75. Grubaugh, N.D., Gangavarapu, K., Quick, J., Matteson, N.L., De Jesus, J.G., Main, B.J., Tan, A.L., Paul, L.M., Brackney, D.E., Grewal, S., et al. (2019). An amplicon-based sequencing framework for accurately measuring intrahost virus diversity using PrimalSeq and iVar. Genome Biol. *20*, 8. https://doi.org/10.1186/s13059-018-1618-7.

76. Garcia-Alcalde, F., Okonechnikov, K., Carbonell, J., Cruz, L.M., Gotz, S., Tarazona, S., Dopazo, J., Meyer, T.F., and Conesa, A. (2012). Qualimap: evaluating next-generation sequencing alignment data. Bioinformatics *28*, 2678–2679. https://doi.org/10.1093/bioinformatics/bts503.

77. Huang, D.W., Sherman, B.T., and Lempicki, R.A. (2009). Systematic and integrative analysis of large gene lists using DAVID bioinformatics resources. Nat. Protoc. *4*, 44–57. https://doi.org/10.1038/nprot.2008.211.